SAND2020-9014R

Estimation of Respirable Aerosol Release Fractions through Stress Corrosion Crack-Like Geometries

Spent Fuel and Waste Disposition

Prepared for
US Department of Energy
Spent Fuel and Waste Science and Technology

S.G. Durbin
E.R. Lindgren
A.G. Perales

Sandia National Laboratories
August 27, 2020
Milestone No. M2SF-20SN010207016
SAND2020-#### R

Sandia National Laboratories is a multimission laboratory managed and operated by National Technology & Engineering Solutions of Sandia, LLC, a wholly owned subsidiary of Honeywell International Inc., for the U.S. Department of Energy's National Nuclear Security Administration under contract DE-NA0003525.

Prepared by
Sandia National Laboratories
Albuquerque, New Mexico 87185 and Livermore, California 94550

Sandia National Laboratories is a multimission laboratory managed and operated by National Technology and Engineering Solutions of Sandia, LLC, a wholly owned subsidiary of Honeywell International, Inc., for the U.S. Department of Energy's National Nuclear Security Administration under contract DE-NA0003525.

ABSTRACT

The formation of a stress corrosion crack (SCC) in the canister wall of a dry cask storage system (DCSS) has been identified as a potential issue for the long-term storage of spent nuclear fuel. The presence of an SCC in a storage system could represent a through-wall flow path from the canister interior to the environment. Modern, vertical DCSSs are of particular interest due to the significant backfill pressurization of the canister, up to approximately 800 kPa. This pressure differential offers a relatively high driving potential for blowdown of any particulates that might be present in the canister. In this study, the carrier gas flow rates and aerosol transmission properties were evaluated for an engineered microchannel with characteristic dimensions similar to those of an SCC. The microchannel was formed by mating two gage blocks with a slot orifice measuring 28.9 μm (0.0011 in.) tall by 12.7 mm (0.500 in.) wide by 8.86 mm (0.349 in.) long (flow length). Surrogate aerosols of cerium oxide, CeO_2, were seeded and mixed inside a pressurized tank. The aerosol characteristics were measured immediately upstream and downstream of the simulated SCC at elevated and ambient pressures, respectively. These data sets are intended to demonstrate a new capability to characterize SCCs under well-controlled boundary conditions. Separate modeling efforts are also underway that will be validated using these data. The test apparatus and procedures developed in this study can be easily modified for the evaluation of more complex SCC-like geometries including laboratory-grown SCC samples.

This page is intentionally left blank.

ACKNOWLEDGEMENTS

This work was funded by the U.S. Department of Energy (DOE), Office of Nuclear Energy Spent Fuel and Waste Disposition Research and Development Program.

The authors would like to express their appreciation to Ned Larson of the DOE for his programmatic leadership and vision. Parallel modeling efforts by Stylianos Chatzidakis at Oak Ridge National Laboratory and Andrew Casella at Pacific Northwest National Laboratory of these tests are eagerly anticipated.

This page is intentionally left blank.

CONTENTS

This page is intentionally left blank.

LIST OF FIGURES

LIST OF TABLES

This page intentionally blank.

ACRONYMS

AED	aerodynamic equivalent diameter
APS	aerosol particle sizer
DCSS	dry cask storage system
DOE	US Department of Energy
DPC	dual-purpose canister
EDM	electrical discharge machining
FCRD	Fuel Cycle Research and Development
FY	fiscal year
HEPA	high-efficiency particulate absorbing
lpm	liters per minute
ORNL	Oak Ridge National Laboratory
PNNL	Pacific Northwest National Laboratory
PSL	polystyrene latex
PWR	pressurized water reactor
SCC	stress corrosion crack
SFWD	Spent Fuel and Waste Disposition
slpm	standard liters per minute
SNF	spent nuclear fuel
SNL	Sandia National Laboratories

This page is intentionally left blank.

ESTIMATION OF RESPIRABLE AEROSOL RELEASE FRACTIONS THROUGH STRESS CORROSION CRACK-LIKE GEOMETRIES

This report fulfills milestone M2SF-20SN010207016 in the Stress Corrosion Cracking and Dry Storage Investigations work package (SF-20SN01020701). This work was sponsored under the Department of Energy's (DOE) Office of Nuclear Energy (NE) Spent Fuel and Waste Disposition (SFWD) campaign.

1 INTRODUCTION

Dry cask storage systems (DCSSs) for spent nuclear fuel (SNF) are designed to provide a confinement barrier that prevents the release of radioactive material, maintain SNF in an inert environment, provide radiation shielding, and maintain subcriticality conditions. SNF is initially stored in pools of water for cooling where the water also provides radiation shielding. As these pools get closer to capacity, dry storage systems are becoming the primary means of extended storage. After sufficient cooling in pools, SNF is loaded into a canister and placed inside a storage cask, where the canister is welded shut. The DCSS is then decontaminated and dried, and the system is moved to an on-site dry storage location. Figure 1.1 shows the major components of a dry storage cask for SNF.

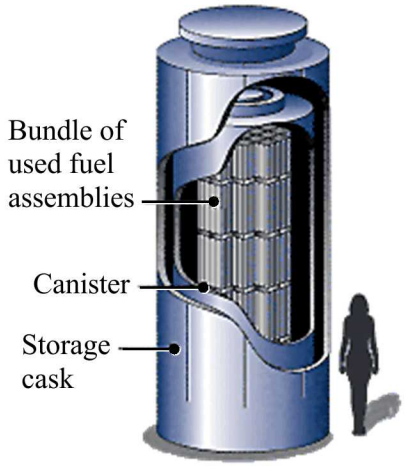

Source: https://www.nrc.gov/waste/spent-fuel-storage/diagram-typical-dry-cask-system.html

Figure 1.1 Typical dry cask storage system.

Typically, the canisters are made of stainless steel. The dry storage system is designed with an open volume between the canister and the storage cask. Rejection of the decay heat is accomplished by air flowing from air inlets at the bottom of the cask to outlets at the top via natural convection. This passively cooled design also allows dust from the environment into the system. These particulates may then collect on the surfaces of the canister. As the SNF cools, salts contained in the dust may deliquesce in the presence moisture from the ambient relative humidity to form concentrated brines, which may contain corrosive species such as chlorides. These species can cause localized corrosion, called pitting. With sufficient stresses, these pits can evolve into stress corrosion cracks (SCCs), which could penetrate through the canister wall and allow communication from the interior of the canister to the external environment [Schindelholz, 2017].

1.1 Objective

The purpose of this on-going research is to explore the flow rates through and the aerosol retention in SCCs. This testing employed engineered slots with characteristic dimensions similar to those in SCCs as analogs. Advanced geometries are being explored for future testing to better approximate SCCs.

Another goal of these tests is to demonstrate improvements to measurement sensitivity and accuracy of the experimental setup. To this end, a new aerosol analysis system, the Palas Promo 3000 HP, has been integrated into the experimental system that can directly monitor aerosol samples at elevated pressures. Furthermore, this high-pressure aerosol characterization system is designed to opto-mechanically switch between monitoring upstream and downstream sensing elements offering nearly simultaneous real-time measurements and eliminating the instrument bias seen in previous testing [Durbin *et al.*, 2018].

1.2 Previous Studies

The data obtainable from the measurement of particulate segregation in flows through open channels has significance in multiple fields. Studies include particle penetration through building cracks [Lewis, 1995, Liu and Nazaroff, 2003, Mosley *et al.*, 2001] to nuclear reactor safety [Powers, 2009], and more recently, storage and transportation of SNF in dry casks. Studies of these systems contribute to the understanding of particulate segregation through small channels as functions of particle size and concentration, channel dimensions, and differential pressures.

Previous work has contributed to the characterization of particulate segregation across channel flow for a range of particle sizes in aerosols. Lewis [Lewis, 1995] was motivated by a lack of empirical studies to support the development of protection factors against solid particles for enclosures. This protection factor was taken as the ratio of the dose of an outside concentration of particulates to the dose accumulated inside an enclosure for a specified time, with the doses defined as concentration-time integrals. Models were derived describing the total transport fraction of particles across a rectangular slot into an enclosure as functions of particle size, differential pressures, and slot heights. Lewis described an experimental apparatus with synthesized aerosols (containing either talc, aluminum oxide, titanium oxide, various silica powders, or ambient dust) mixed in a chamber containing an enclosure with a rectangular slot open to the chamber. A differential pressure was established between the chamber and the enclosure. Protection factors were found by comparing mass concentration values inside and outside the enclosure over a given time. The primary observations here were the decrease in total transport fraction with increasing particle size from 1-10 μm as well as a decrease in protection factor (corresponding to an increase in total transport fraction) with increasing differential pressures and slot heights.

Liu and Nazaroff [Liu and Nazaroff, 2003] conducted experiments of aerosol flow through rectangular slots using various building materials, including aluminum, brick, concrete, and wood. The slot heights were 0.25 mm and 1 mm, which are large compared to the micron- to submicron-sized particles they flowed through the cracks. They obtained data for particle penetration (defined as the ratio of downstream to upstream particle concentration), related to total transport fraction, as a function of particle size. They found that, for 0.25 mm cracks, particle sizes between 0.1-1 μm achieved penetration factors near unity, while smaller and larger particles showed diminished penetration factors for pressure differentials of 4 and 10 Pa. Meanwhile, for 1 mm slot heights, the penetration factors were near unity for the majority of the particle size distribution. Their results matched closely with models they created from analysis of particle penetration through simplified cracks [Liu and Nazaroff, 2001] and had similar qualitative conclusions to Lewis's work.

Mosley studied particle penetration through a 0.508 mm slot height between aluminum plates with particles of aerodynamic equivalent diameters (AED) from 0.1 to 5 μm [Mosley *et al.*, 2001]. They found penetration factors close to unity for particle sizes between 0.1-1 μm, with a sharp drop-off in penetration factor for particle sizes larger than 1 μm for pressure differentials between 2 and 20 Pa – this was

consistent with Liu and Nazaroff's results when considering the order of magnitude of the pressure differentials and particle size distributions.

The motivation behind the above work was based on ambient particle penetration of enclosures and the amount of particles subject to human exposure, with slot heights and pressure differentials corresponding to conditions typically associated with building cracks and pressure differences between indoor and outdoor environments, respectively. However, the channel dimensions considered do not apply to the channel geometry associated with SCCs from potential corrosion of dry casks. The literature reports typical crack heights to be around 16 to 30 μm [EPRI, 2014 & 2017; Meyer *et al.*, 2016] and internal pressures of 100 to 760 kPa (14.5 to 110 psig) [EPRI, 2017] for a range of cask models. Therefore, an apparatus and procedures were developed to investigate a slot height on the order of 10 μm and pressure differentials on the order of 100 kPa to supplement the established database of particulate transmission in microchannel flows. This experimental approach is intended to be adaptable for future testing of more prototypic stress corrosion crack geometries. Preliminary results indicated 44% of the aerosols available for transmission were retained upstream of the microchannel [Durbin *et al.*, 2018].

1.3 Current Study

An aerosol spectrometer is utilized for this study to measure the size resolved aerosol concentration, also known as aerosol size distribution. The instrument selected for this study is ideally suited for pressurized operation and has eliminated previously observed instrument biases [Durbin *et al.*, 2018]. The Palas Promo 3000 is fiber-optically coupled to two Welas 2200 high pressure aerosol sensors. The high-pressure aerosol sensor directly samples gas streams at native pressures up to 1.0 MPa. Rapid fiber optic switching allows a single instrument to analyze the upstream and downstream aerosol sensors in quasi-simultaneous fashion using the same optical detector. Thus, instrument bias was eliminated, and sample line losses were substantially minimized.

This page intentionally blank.

2 APPARATUS AND PROCEDURES

The experimental approach adopted for these studies is similar to previous studies [Lewis, 1995; Mosley *et al.*, 2001; and, Liu and Nazaroff, 2001 and 2003] in that aerosol analyzers are used to characterize the particle size distribution and concentration present in the gas before and after flowing through a simulated crack. Because these previous studies considered aerosol transport through building walls or containment structures, the focus was on flows through relatively wide and long slots driven by constant low pressure drops. In the present study, consideration was given to aerosol transport through dry storage canister walls. Here, the focus was on much narrower and shorter microchannels that represent stress corrosion cracks through the canister wall driven by initially higher pressure drops.

Two types of tests were considered for these studies. In the first test type denoted as a "blowdown," the storage tank was pressurized, sealed from the pressure source, and allowed to blowdown to ambient pressure via the microchannel. In the second test type denoted as "constant pressure," the pressure in the storage tank was maintained at a constant value with a pressure controller as flow is directed through the microchannel. The blowdown type of test more closely simulated the expected behavior of a pressurized SNF canister. While not prototypic, the constant pressure tests decoupled the pressure transient, which allowed better examination of the SCC discharge characteristics as it was fouled with deposited particulates.

2.1 General Construction

The general layout of the experimental setup is illustrated in Figure 2.1 and Figure 2.2. A 0.908 m^3 (240 gal) pressure tank is used to simulate the canister. The tank was loaded with a measured quantity of dry powder aerosols using a Palas rotating brush generator (RBG) and then pressurized. Flow leaving the test section and exhausting to ambient was measured as was the flow drawn into each of the aerosol sensors. The engineered microchannel, simulating a crack, was mounted in the middle of the test section comprised of mounting flanges and two 0.61 m (24 inch) long, 0.10 m (4 inch) diameter schedule 40 pipe nipples. A sample stream was drawn from the centerline at the nipple midpoint on the high-pressure upstream and low-pressure downstream sides of the test microchannel for aerosol size and concentration characterization using identical Welas 2200 high pressure aerosol sensors monitored by a single Palas Promo 3000 HP analyzer. Mass flow meters measured the sample flow leaving each of the aerosol sensors. Flow from the tank and through the test section was measured by a mass flow meter downstream of the test section. Pressure was monitored on the upstream and downstream sides of the microchannel using pressure transducers. A low pressure drop, high-efficiency particulate absorbing (HEPA) filter was used to remove all aerosols from the exhaust stream before the final mass flow measurement.

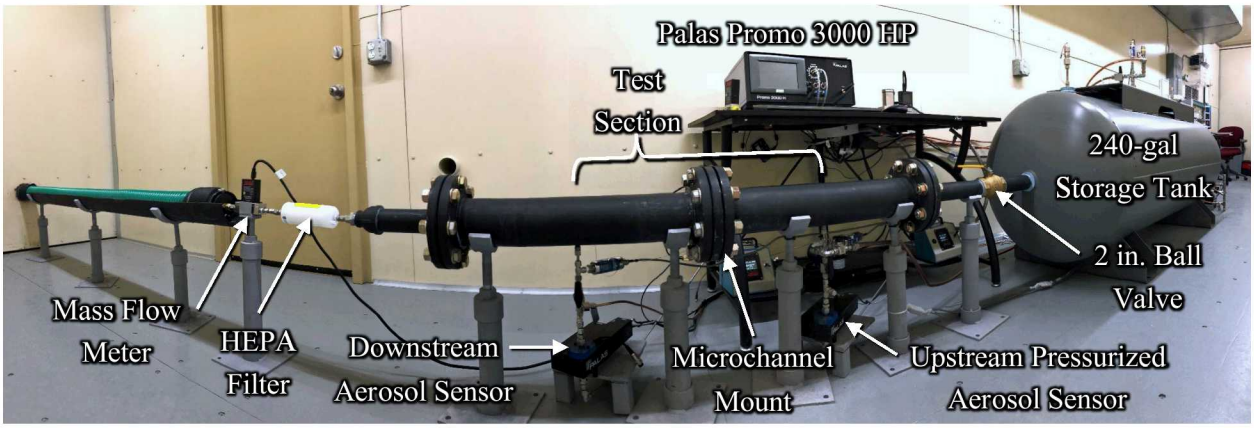

Figure 2.1 General layout of the experimental apparatus.

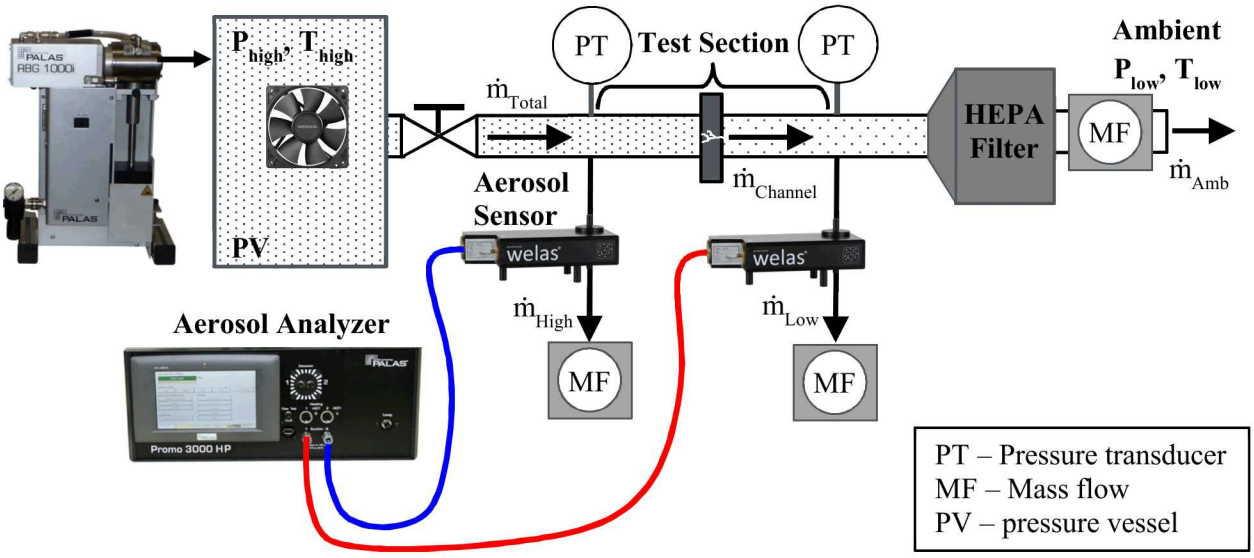

Figure 2.2 Schematic of the apparatus showing the major components.

2.2 Design of the Microchannel

2.2.1 Simple Slot Orifice

An engineered microchannel has been fabricated from paired high-precision Mitutoyo gage blocks. The microchannel was machined into the surface of one gage block using electrical discharge machining (EDM). The mounting holes were also cut using wire EDM. As shown in Figure 2.3 the dimensions of the microchannel are 12.7 mm (0.500 in.) wide, 8.86 mm (0.349 in.) long and an average of 28.9 µm (0.0011 in.) deep. The paired halves of the gage blocks are bolted together to form the microchannel held in a mounting assembly as detailed in Figure 2.4. An isometric view of the microchannel mounted to the flow flange is shown in Figure 2.5.

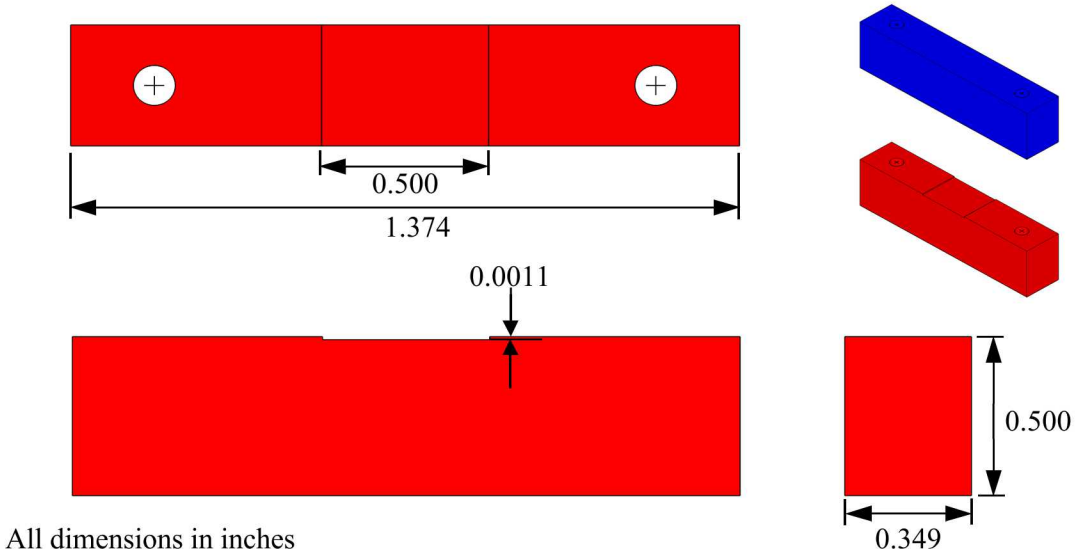

Figure 2.3 Schematic of the microchannel assembly.

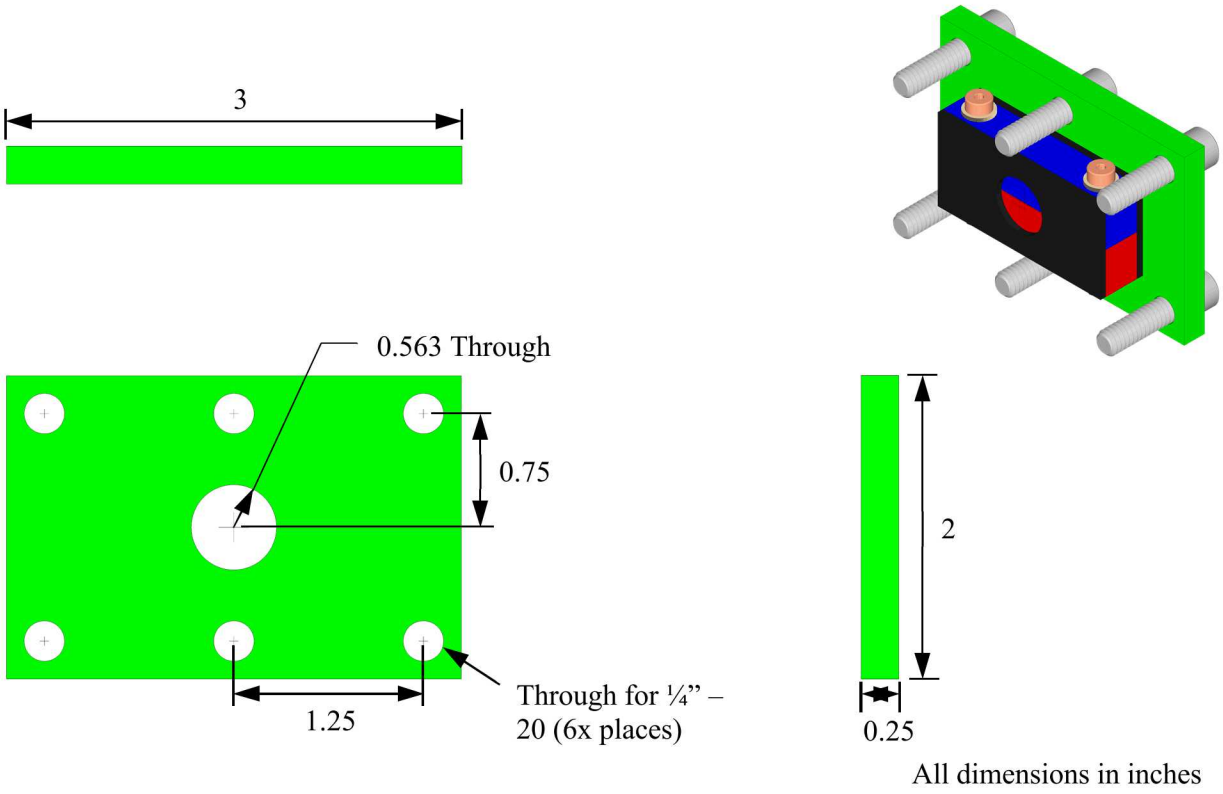

Figure 2.4 Details of the microchannel mounting assembly.

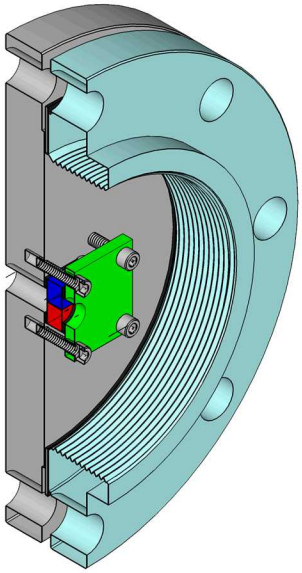

Figure 2.5 Isometric cutaway showing the microchannel mounted to the flow flange.

Figure 2.6 shows profilometry of the microchannel on both sides of the as-built microchannel. These scans represent approximately 1.2 mm (0.047 in.) of the overall 12.7 mm (0.500 in.) slot, or 9%. The average step height based on these measurements is 28.9 µm (0.0011 in.). These profiles were taken with a Keyence VK-X100 laser scanning microscope.

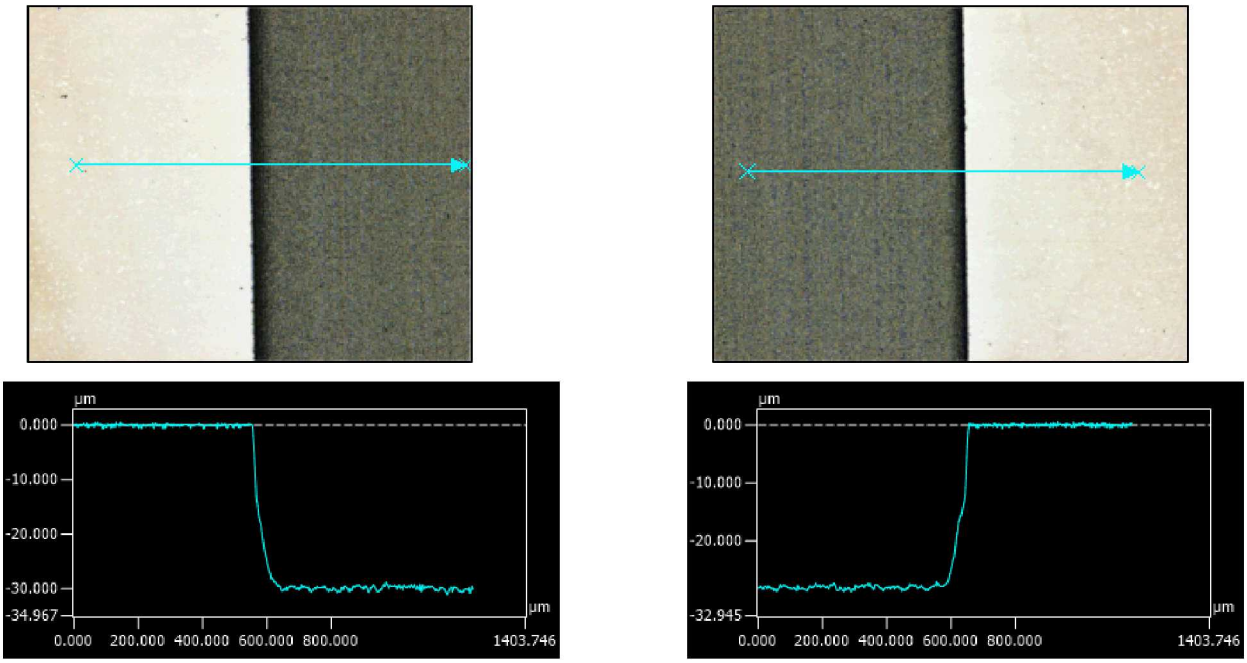

Area average step height: 29.9 µm

Area average step height: 27.9 µm

Figure 2.6 Profilometry of the microchannel orifice.

During the profilometry, the surface roughness of the microchannel was also characterized with the Keyence VK-X100 laser scanning microscope. The results of the surface roughness characterization are given in Figure 2.7. In the embedded tables, S_a is the arithmetical mean height of the shown areas and is defined as the average of the difference between each surface point measurement and the mean plane of the surface. The root mean square height, S_q, is equivalent to the standard deviation of heights. Area2 is the microchannel surface and Area1 is the adjoining gage surface. By all measures the surface roughness of the microchannel was roughly twice that of the gage block surface.

Left Side 10×

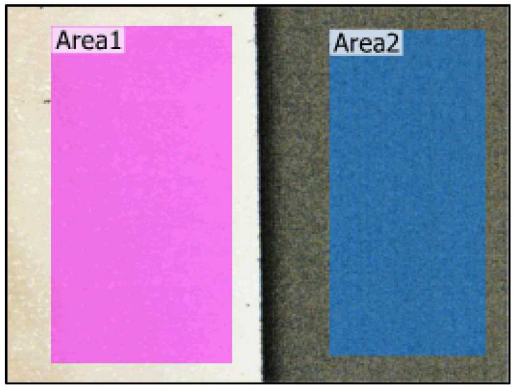

	S_a (µm)	S_q (µm)
Area1	0.213	0.275
Area2	0.408	0.520

Right Side 10×

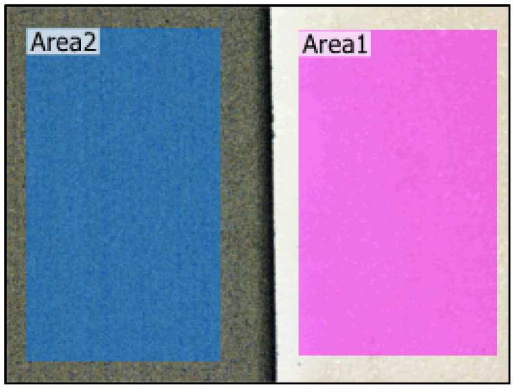

	S_a (µm)	S_q (µm)
Area1	0.238	0.300
Area2	0.386	0.494

Figure 2.7 Surface roughness characterizations.

A visualization of the discharge flow through the microchannel is shown in Figure 2.8. In this image, the mounting flange has been reversed and mounted to the upstream nipple with the downstream nipple removed. The microchannel is mounted on the bottom half and much of the flow was noted to exit the orifice in an upwardly angled jet.

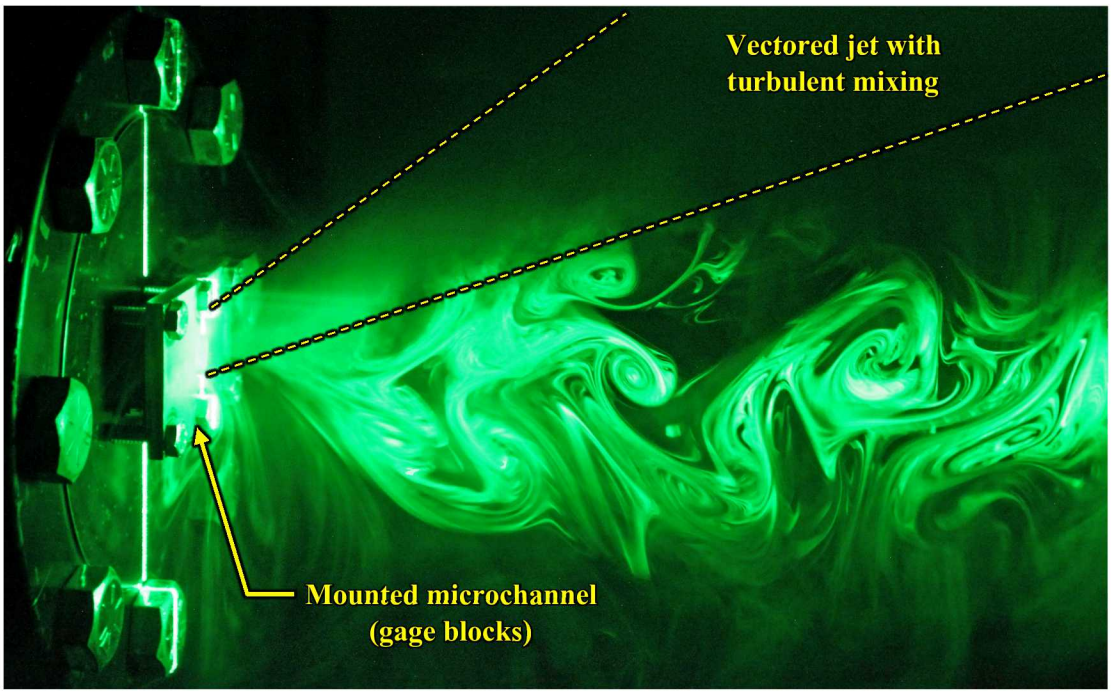

Figure 2.8 Flow visualization of the microchannel flow.

2.3 Instrumentation

The following instrumentation was used to characterize these tests. All stated uncertainties are assumed to represent 95% confidence intervals unless otherwise stated.

2.3.1 Pressure

Pressure was monitored on the upstream side using a 1,034 kPa (150.0 psia) Setra Model ASM transducer and on the downstream side with a 103 kPa (15.0 psia) Model ASM transducer. The pressure in the tank was monitored with a 2,068 kPa (300 psia) Setra Model ASM transducer.

The uncertainty of all the Setra pressure transducers is < ± 0.05% full scale (FS).

Table 2.1 Summary of pressure transducers.

Location	Model No.	Full Scale (kPa)	Uncertainty (kPa)
Storage tank	ASM1-300P-A-1M-2C-03-A-01	2,068	1.03
Upstream	ASM1-150P-A-1M-2C-03-A-01	1,034	0.52
Downstream	ASM1-015P-A-1M-2C-03-A-01	103	0.05

2.3.2 Temperature

All temperature measurements were taken with K-Type thermocouples with standard calibration. The suggested, combined uncertainty in these measurements including data acquisition, cabling, and positioning errors is 1% of the reading in Kelvin.

2.3.3 Mass Flow Rate

Flow from the test section was measured by a low pressure drop mass flow meter (Alicat, MW-20SLPM for $\Delta P \approx 420$ kPa and 720 kPa, and MW-2SLPM for $\Delta P \approx 120$ kPa). The standard liter per minute (slpm) is defined as one liter of air flow at standard conditions of 101.325 kPa and 25 °C (*i.e.* reference density of $\rho_{STP} = 1.184$ kg/m^3). Because the volumetric flow rate, Q_{STP}, is referenced to a fixed standard temperature and pressure, it may also be used as a mass flow rate, where the mass flow rate is defined as $\dot{m} = Q_{STP} \times \rho_{STP}$. A conversion of units is necessary to convert between the values for Q_{STP} and $\dot{m}$ reported in Table 2.2.

For all the mass flow meters and controllers, the reported 95% uncertainty is ± (0.4% of reading + 0.2% FS) for a maximum of ± 0.6% FS.

Table 2.2 Summary of mass flow instrumentation.

Description	Model No.	Full Scale Q_{STP} (slpm)	Full Scale $\dot{m}$ (kg/s)	Uncertainty (kg/s)
High flow ambient exhaust	MW-20SLPM	20	3.9×10^{-4}	2.4×10^{-6}
Low flow ambient exhaust	MW-2SLPM	2	3.9×10^{-5}	2.4×10^{-7}
High pressure aerosol sensor	MC-5SLPM	5	9.9×10^{-5}	5.9×10^{-7}
Low pressure aerosol sensor	MC-5SLPM	5	9.9×10^{-5}	5.9×10^{-7}

2.3.4 Aerosol Spectrometer

The Palas Promo 3000 HP is a flexible, light-scattering aerosol spectrometer system that uses twin sensors to determine quasi-simultaneous particle concentration and particle size at two locations. Fiber-optic cables (light wave conductor or LWC) are used to carry light from the main controller to the remote Welas 2200 high pressure aerosol sensors as well as the resulting light-scattering signal from the remote sensors back to the main controller. The Welas 2200 sensors are specially designed to require only 0.5 actual liters per minute (lpm) of flow. This high-pressure aerosol sensor is capable of directly measuring samples at pressures up to 1000 kPa. Rapid fiber optic switching allows a single instrument to analyze the upstream and downstream aerosol sensors in quasi-simultaneous fashion.

The instrument collected data from the upstream sensor for 50 seconds in ten-second increments, generating five upstream data points. The switch to the downstream sensor required ten seconds, and then the instrument collected data from the downstream sensor generating another five downstream data points. The nature of the data stream is therefore a series of five data points at 10 second intervals followed by a 60 second gap in data while the other sensor was analyzed.

The aerosol spectrometer characteristics are summarized in Table 2.3. This sensor range makes reliable measurements possible over a concentration range from 1 to 10^6 particles/cm^3. The instrument is ideally suited to simultaneously monitor the aerosols from the high-pressure upstream and low-pressure downstream side of the simulated crack for aerosol size and concentration characteristics.

Table 2.3 Summary of the aerosol spectrometer capabilities.

Instrument Characteristic	Value
Aerosol size range	0.3 to 17 µm
Aerosol size channels	64/decade
Minimum Particle Concentration	1 particle/cm^3
Maximum Particle Concentration	10^6 particles/cm^3
Maximum Sample Pressure	1,000 kPa
Maximum Sample Temperature	120 °C

2.3.5 Aerosol Generator

The aerosols were loaded into the pressure tank with a Palas rotating brush generator RBG 1000 (Figure 2.9*a*). The RBG 1000 can deliver particles at a rate between 40 mg/h to 430 g/h at pressures up to 300 kPa. The heart of the instrument is the rotating brush (Figure 2.9*b*). The desired aerosols to be dispersed are packed into a cylinder. A transport piston slowly pushes the bed of packed powder into the rotating metal bristle brush that dislodges particles and holds them in the bristles. When the brush rotates 180 degrees further, the bristles are exposed to a flow of dispersion carrier gas that suspends the particles and transports them away.

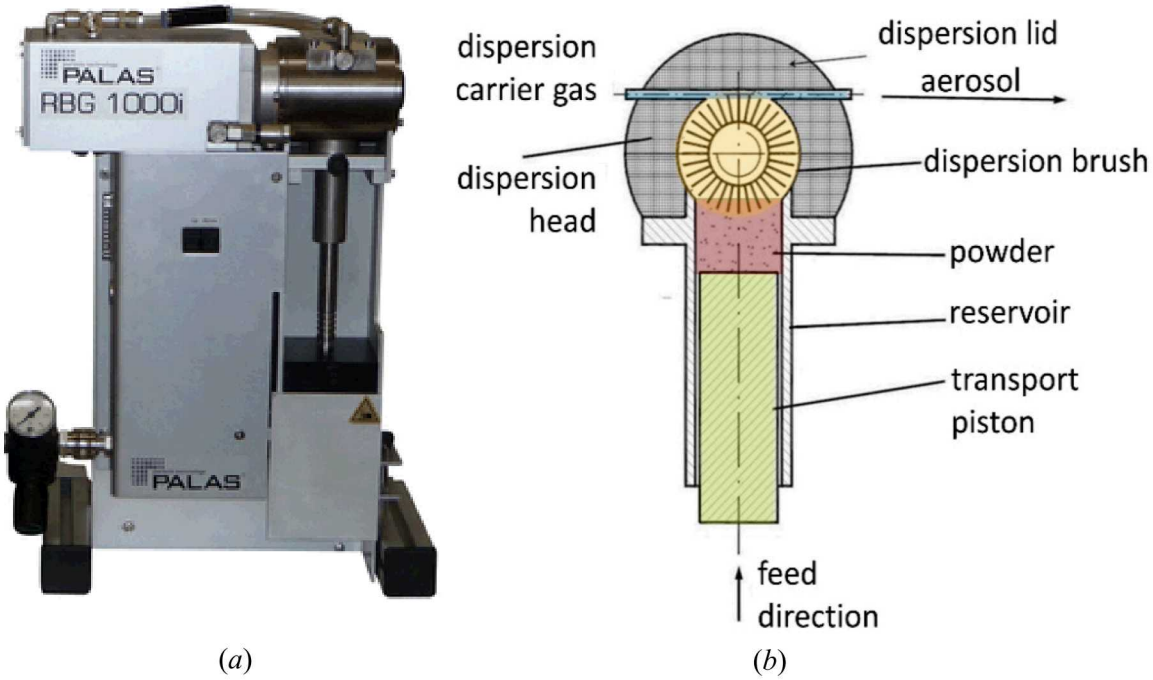

Figure 2.9 (*a*) Image of the Palas RBG 1000i and (*b*) diagram of the rotating brush. [Palas GmbH, RBG 1000 Particle Generator Manual, Karlsruhe, Germany, 2002]

2.4 Aerosol Characteristics

2.4.1 Selection of Surrogates

Cerium oxide (CeO_2) was chosen as the surrogate for spent nuclear fuel ($\rho_{SNF} \approx 10$ g/cm^3) because of its relatively high density ($\rho_{CeO2} = 7.22$ g/cm^3) and its commercial availability. For cerium oxide, an aerodynamic equivalent diameter (AED) particle of 10 µm equates to a geometric particle size of 3.72 µm. Geometric particle size is used exclusively through the remainder of this report. Figure 2.10 shows the particulate sizes as characterized by the probability distribution function (PDF) and cumulative distribution function (CDF) of the surrogate used in these tests. Here, the distributions are plotted as a function of geometric diameter (bottom) and AED (top). This specific lot of CeO_2 was chosen because the particulates were concentrated in the respirable range (AED < 10 µm). The mass median diameter (MMD) was 2.4 µm (or $MMD_{AED} = 6.4$ µm), the geometric standard deviation (GSD) was 1.9, and ~75% by mass of the particles was respirable (AED < 10 µm). Fifty percent of the measured particles have a mass smaller than the MMD (also known as D_{50}), and 50% of the measured particles have a mass that is greater.

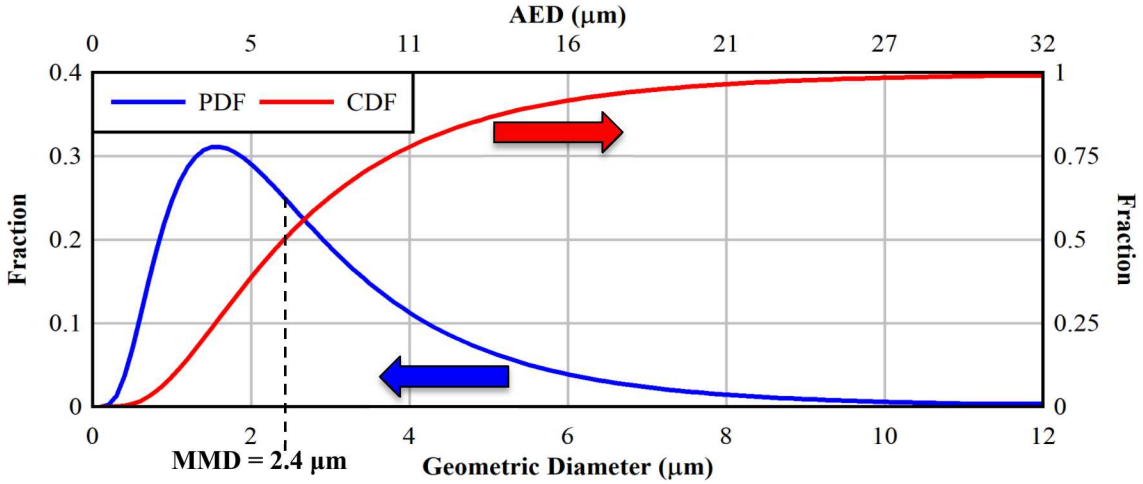

Figure 2.10 Size distributions of the cerium oxide surrogates used in testing.

2.4.2 Reference Initial Aerosol Concentration

The particulates released from SNF were characterized when air was forced through segmented fuel [Hanson *et al.*, 2008]. The geometric particle size data from nine tests conducted on four fuel rod segments are summarized in Figure 2.11. The average of the nine tests yielded an MMD of 3.46 µm (geometric diameter), a GSD of 2.24, a total release fraction of 1.9×10^{-5} of which 46% was respirable for a respirable release fraction of 8.9×10^{-6}. This respirable release fraction is in reasonable agreement with 4.8×10^{-6} cited in NUREG-2125 [NRC, 2012] and 3×10^{-6} cited in SAND90-2406 [Sanders, *et al.*, 1990].

To estimate an upper aerosol density for spent fuel dry storage, a canister with 37 pressurized water reactor (PWR) assemblies with a fuel mass (UO_2) 520 kg per assembly was assumed. One percent of the fuel was assumed to fail simultaneously due to an undefined event. The canister was assumed to have an internal free volume of 6 m^3 and a starting initial pressure of 800 kPa (116 psia). The equivalent aerosol density for this assumed system at standard temperature and pressure (STP) is approximately $C_{m,\,STP} = 54$ mg/m^3. For all testing described in this paper, the standard temperature and pressure were taken as the default values for the mass flow rate instruments (Alicat MC and MW Series) of 298.15 K (25 °C) and 101.353 kPa (14.7 psia).

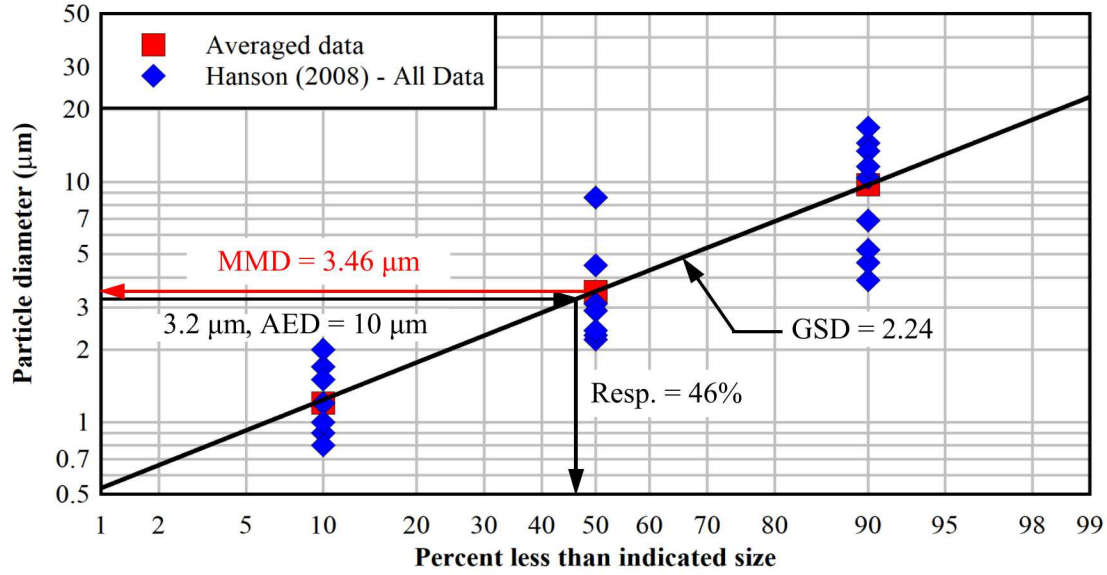

Figure 2.11 Respirable fraction of spent fuel from Hanson *et al.* 2008.

3 RESULTS

3.1 Clean Flow Tests

The flow characteristics of the engineered microchannel used in this study were first evaluated in the absence of aerosols. Table 3.1 lists the clean, aerosol-free tests that have been conducted. For the two tests conducted with the Promo "On," sample flows were drawn through the upstream and downstream aerosol sensors as in the aerosol-laden tests. The flow results of these tests are summarized in Figure 3.1, which shows the mass flow rate through the clean microchannel as a function of a wide range of pressure drops. These data are an accumulation of all the clean tests conducted to date. Two mass flow meters were used for the testing with different full-scale ranges of 3.9×10^{-5} and 3.9×10^{-4} kg/s and uncertainties of 2.4×10^{-7} and 2.4×10^{-6} kg/s, respectively. The increased noise in mass flow rate from 2×10^{-6} to 1×10^{-5} kg/s represents the accuracy limit of the higher-range mass flow meter. Also shown for reference are the three initial pressure drops considered in the aerosol-laden tests: nominally 120 kPa, 420 kPa, and 720 kPa.

Table 3.1 Aerosol-free flow test matrix.

Date	Geometry	Test Type	Promo	ΔP_o (kPa)
3/19/2020	Slot	Clean Blowdown	Off	715
3/20/2020	Slot	Clean Blowdown	Off	724
3/24/2020	Slot	Clean Blowdown	Off	127
4/10/2020	Slot	Clean Blowdown	Off	718
4/14/2020	Slot	Clean Blowdown	Off	127
4/9/2020	Slot	Clean Blowdown	On	729
4/10/2020	Slot	Clean Blowdown	On	122

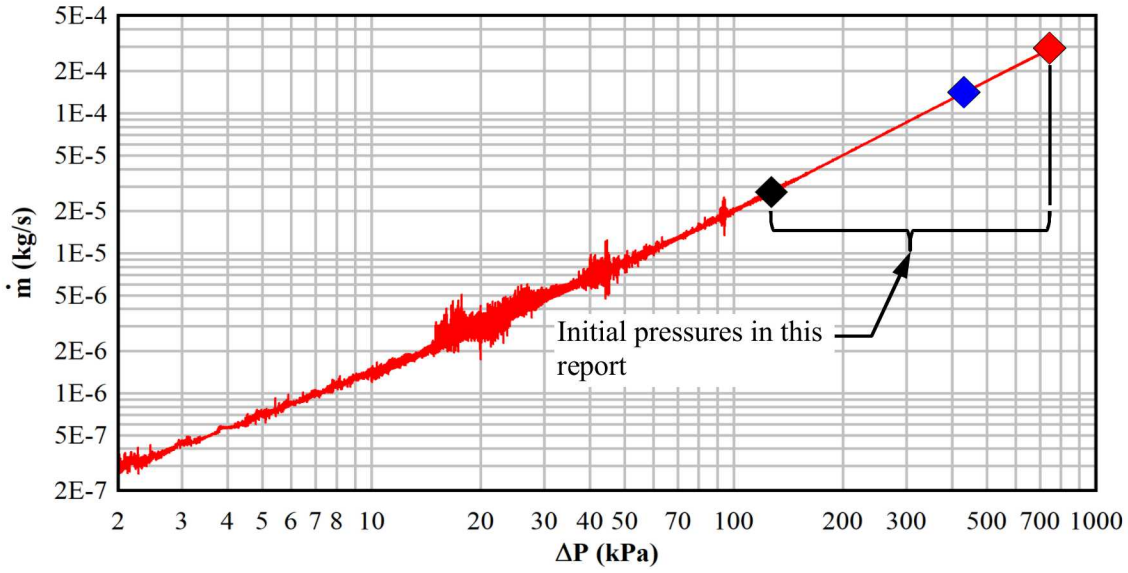

Figure 3.1 Mass flow rate as a function of pressure drop across the microchannel.

3.2 Aerosol-Laden Flow Tests

As summarized in Table 3.2, a total of twenty-two aerosol-laden air flow tests were conducted with three nominal initial pressure drops (120 kPa, 420 kPa, and 720 kPa) each for two test modes (blowdown and constant pressure) over a wide range of initial upstream aerosol concentrations (1.3 mg/m^3 to 168 mg/m^3). The final, integrated aerosol mass, M(τ), in the upstream and downstream sections are given for each test. In addition, the ratio of these values is reported as the integrated transmission. The methods for determining these values are defined in the next section.

Table 3.2 Aerosol-laden flow test matrix summary of results.

			Upstream Initial Conditions				Final		
Date	Test Mode	ΔP_o (kPa)	C_m (mg/m^3)	$C_{m,STP}$ (mg/m^3)	MMD (μm)	GSD	M_{Down} (mg)	M_{Up} (mg)	Integrated Transmission
4/29/2020	Blowdown	121	163.0	80.7	2.3	2.0	2.14	4.55	0.470
4/23/2020	Blowdown	125	100.6	49.2	2.6	1.9	1.23	2.95	0.416
5/27/2020	Constant Press.	116	124.6	62.1	2.1	1.8	1.69	3.92	0.432
6/3/2020	Constant Press.	120	109.6	54.7	2.5	2.0	1.30	2.78	0.468
6/9/2020	Constant Press.	118	28.9	14.3	2.3	2.0	0.46	0.94	0.489
7/1/2020	Constant Press.	118	4.0	2.0	2.2	1.9	0.08	0.14	0.546
7/24/2020	Blowdown	417	16.6	3.4	2.0	2.2	0.69	1.57	0.440
7/17/2020	Blowdown	417	4.4	0.9	2.2	2.0	0.14	0.40	0.352
7/23/2020	Blowdown	417	4.3	0.9	2.0	2.0	0.14	0.37	0.393
7/6/2020	Constant Press.	418	167.8	33.5	2.7	2.0	5.15	13.0	0.396
7/22/2020	Constant Press.	417	58.8	11.7	2.6	2.1	1.72	5.05	0.340
7/8/2020	Constant Press.	417	21.7	4.3	2.7	2.0	0.62	1.47	0.421
7/20/2020	Constant Press.	417	5.6	1.1	2.3	2.1	0.17	0.45	0.366
7/16/2020	Constant Press.	417	2.9	0.6	1.9	2.1	0.14	0.32	0.429
7/15/2020	Constant Press.	417	1.3	0.3	2.7	1.9	0.03	0.08	0.366
5/5/2020	Blowdown	726	153.3	19.6	2.3	2.1	7.40	18.3	0.404
4/20/2020	Blowdown	740	104.2	13.0	2.1	2.2	2.51	7.63	0.329
7/29/2020	Blowdown	714	22.9	2.9	2.0	2.3	1.25	3.27	0.384
5/20/2020	Constant Press.	713	146.4	18.3	4.7	2.7	6.74	14.3	0.470
6/24/2020	Constant Press.	713	12.4	1.5	3.7	2.1	0.42	1.22	0.344
6/29/2020	Constant Press.	715	4.9	0.6	3.3	2.1	0.16	0.42	0.377
6/18/2020	Constant Press.	715	4.7	0.6	2.5	2.2	0.21	0.57	0.370

3.2.1 Data Analysis

The measured instantaneous mass rate of aerosols upstream or downstream of the microchannel at any time t may be expressed as shown in Equation 3.1. Here, the mass flow rate, Q_{STP}, at time t is multiplied by the mass concentration of aerosols, $C_{m,STP}$, at the same time t, both at STP conditions. The instantaneous transmission at time t is defined as the mass rate downstream divided by the corresponding instantaneous mass rate upstream as shown in Equation 3.2. The integrated mass transmitted to and from the microchannel is calculated as the integral of the instantaneous mass rate from a lower limit of t_o = 0.1 hours to an upper limit governed by the available aerosol data (τ) as shown in Equation 3.3. The initial

offset in the integration limit of 0.1 hours is to account for the short delay in flow of aerosols from the storage tank into the test section. By taking the ratio of the downstream to the upstream integrated mass of aerosols, the integrated transmission of aerosols through the microchannel may be estimated (Equation 3.4). Because the mass flow of gas through the microchannel is conserved in the upstream and downstream calculation in Equation 3.1, the flow cancels in the calculation of the integrated transmission in Equation 3.4.

$$m(t) = Q_{STP}(t) \cdot C_{m,STP}(t) \text{ [Units = mg/s]} \quad \textbf{3.1}$$

$$\text{Instantaneous Retention} = 1 - m_{Down}(t) / m_{Up}(t) \quad \textbf{3.2}$$

$$M(\tau) = \int_{t_o}^{\tau} m(t)\,dt \text{ [Units = mg]} \quad \textbf{3.3}$$

$$\text{Integrated Transmission} = M_{Down}(\tau) / M_{Up}(\tau) \quad \textbf{3.4}$$

3.2.2 Aerosol Concentration

Transmission of particulates through the microchannel was determined directly by measuring the aerosol concentration contemporaneously both upstream and downstream of the microchannel. To facilitate this analysis, the raw temporal concentration data were fit to a fourth order log-log polynomial. Figure 3.2 shows an example of the upstream and downstream concentration transients and curve fits for the constant pressure test conducted on July 6, 2020. The upstream aerosol concentration drops three orders of magnitude over twelve hours indicating aerosol depletion in the pressure tank. The concentration of aerosol for any given time is greater upstream than downstream indicating the microchannel was acting as a filter. The concentration difference between upstream and downstream is greatest initially and the two concentrations asymptotically approach each other at later times. For all tests, the start of the test (t = 0 hours) is marked by the opening of the 2 in. ball valve to the storage tank releasing aerosols to the microchannel. An additional, temporal correction was needed to synchronize the samples because of the transit time of the carrier gas from the upstream to the downstream sample ports. This correction was approximated by shifting the downstream data earlier in time based on the time required to displace the volume of gas between the upstream sampling port and the microchannel.

Figure 3.4 shows a typical result of the integrated aerosol masses for the upstream and downstream sections on the left dependent axis for the test conducted on July 6, 2020. The ratio of the downstream to the upstream aerosol mass, *i.e.* integrated transmission, is shown on the right dependent axis. Although care was taken to accommodate the stabilization of the aerosol concentrations at the start of the test, the combination of curve fitting and the selection of a test-independent lower integration limit, t_o = 0.1 h, led to some integrated transmissions displaying initial, non-monotonic behavior.

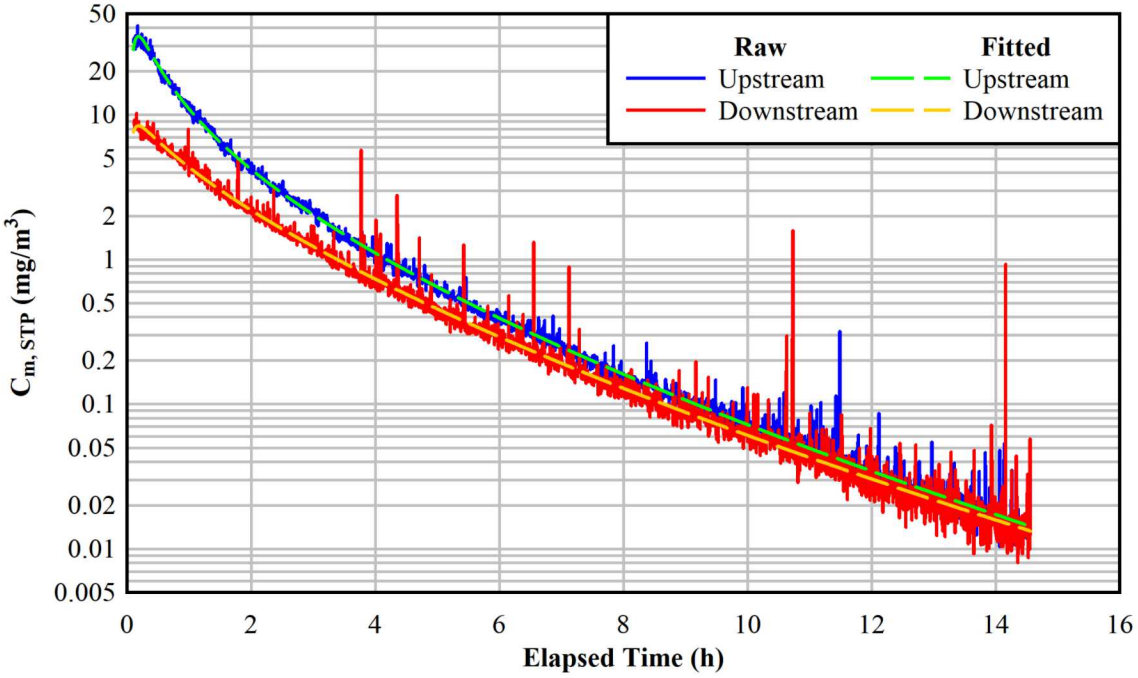

Figure 3.2 Raw and curve-fit aerosol mass concentrations for the test on 07/06/2020 with a constant ΔP = 420 kPa and an initial upstream concentration of $C_{m,\,Up,\,STP,\,o}$ = 33.5 mg/m^3 ($C_{m,\,Up,\,o}$ = 167.8 mg/m^3).

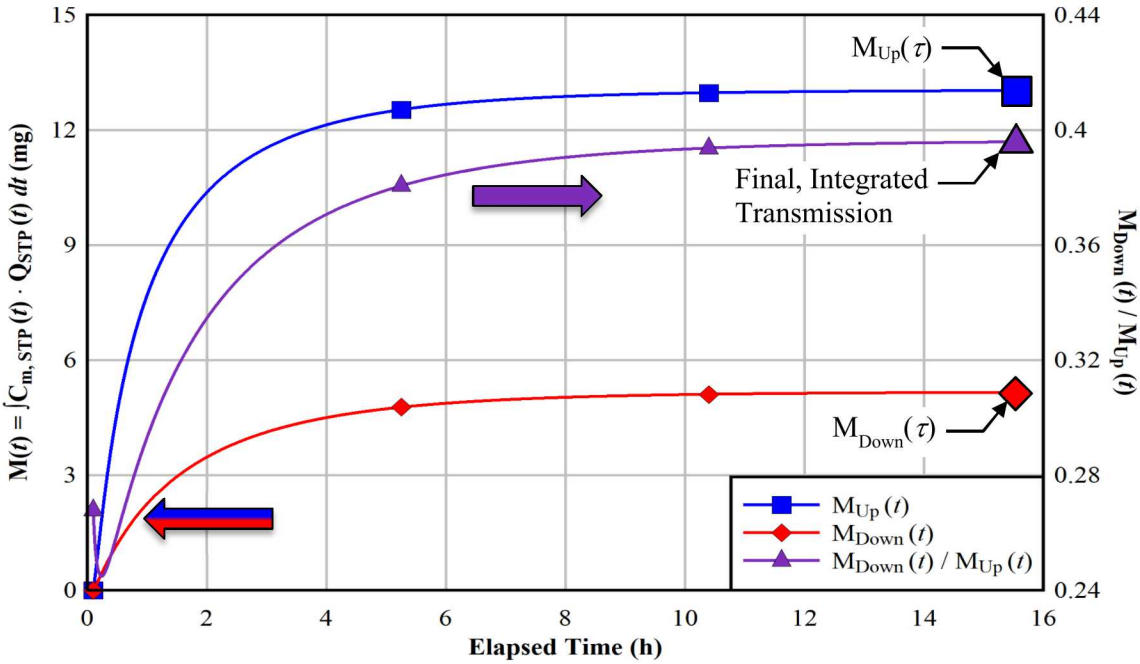

Figure 3.3 Integrated aerosol mass concentrations for the test on 07/06/2020 with a constant ΔP = 420 kPa and an initial upstream concentration of $C_{m,\,Up,\,STP,\,o}$ = 33.5 mg/m^3 ($C_{m,\,Up,\,o}$ = 167.8 mg/m^3).

3.2.3 Normalized Transient Mass Flow for Constant Pressures

The normalized mass flow of particle laden gas through the microchannel as a function of time for nominal constant pressure drops of 120 kPa, 420 kPa, and 720 kPa are shown in Figure 3.4, Figure 3.5, and Figure 3.6, respectively. All three plots are parameterized by aerosol mass concentration. The color of data for each curve presented is mapped to the concentration level with red being the highest (100 to 500 mg/m^3) and dark blue the lowest (0.1 to 5 mg/m^3). This convention is used throughout the remainder of this report unless otherwise noted. Error bars indicate the experimental uncertainty in the measurements.

At a pressure drop of nominally 120 kPa as shown in Figure 3.4, there is a clear correlation between flow rate and aerosol concentration. Each curve shows an initial rapid drop in flow rate followed by a slow asymptotic approach to a steady state level that may indicate restriction of flow through the channel. Increasing the aerosol concentration leads to a decreasing final, steady-state normalized flow. A sharp increase is noted in the normalized flow rate at ~3.25 h for the test conducted with $C_{m, Up, o}$ = 109.6 mg/m^3. Review of the test data did not reveal any abrupt events. Given that this increase is less than the uncertainty of the measurement, no significance is assigned to this event.

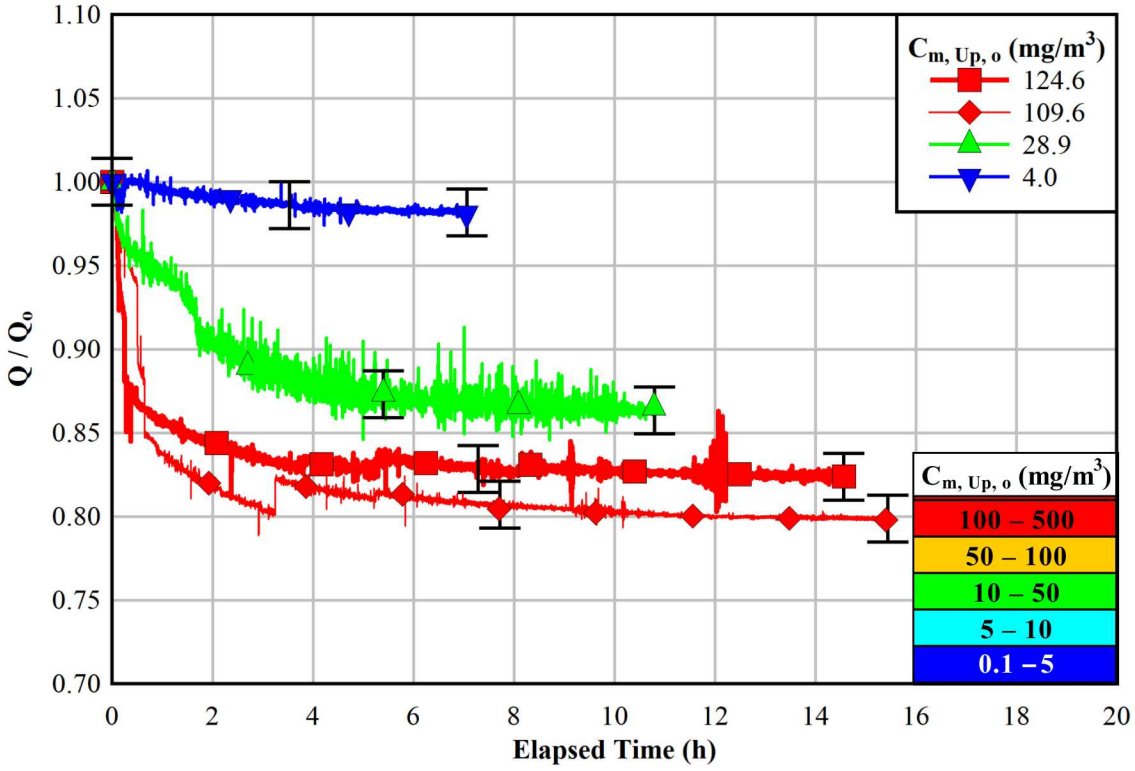

Figure 3.4 Normalized channel gas mass flow rate for constant pressure testing at ΔP ≈ 120 kPa as a function of time.

The flow behavior is different at the two higher pressure drops. For the constant pressure drop at nominally 420 kPa and 720 kPa, the flow does not correlate with aerosol concentration and remains about the same throughout the tests as shown in Figure 3.5 and Figure 3.6, respectively. Post-test visual inspections indicate variable aerosol deposition quantities and patterns in the microchannel for similar initial mass concentrations at different pressure differentials. The 120 kPa tests appeared to show higher levels of aerosol deposition in the microchannel. These visual observations were strictly qualitative in nature. These blockages, while present, do not appear to significantly affect the flow rate for the two higher pressure differentials.

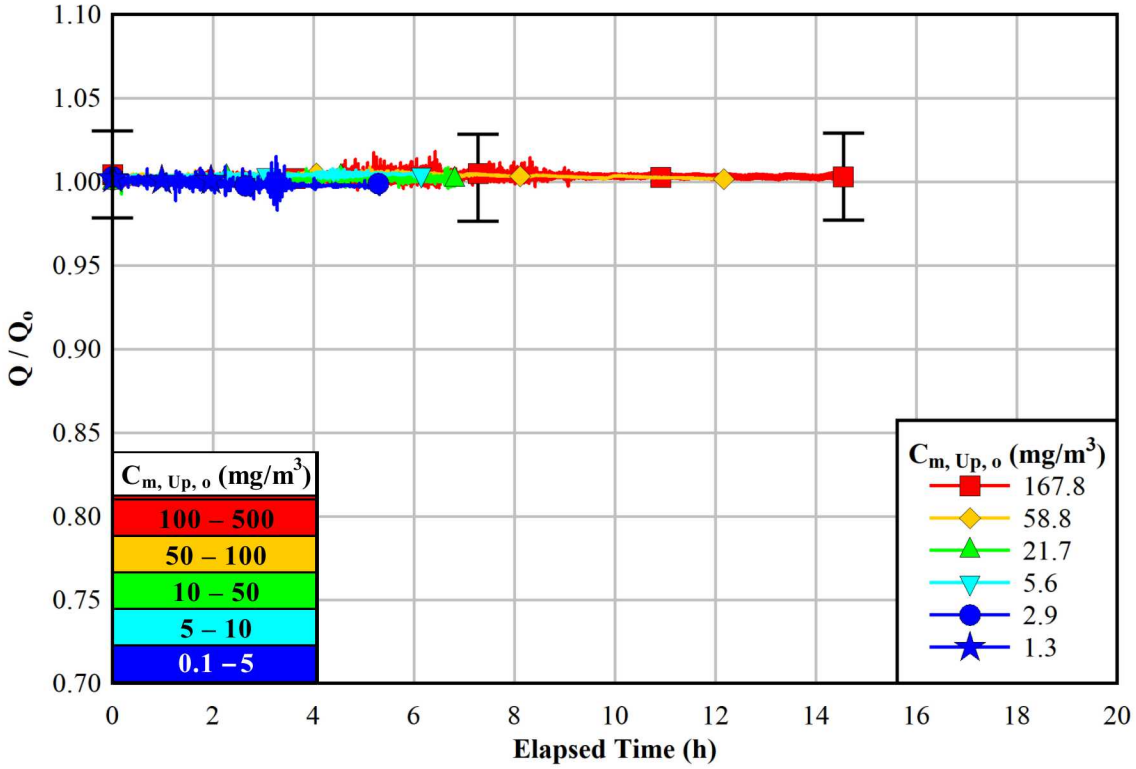

Figure 3.5 **Normalized channel gas mass flow rate for constant pressure testing at ΔP ≈ 420 kPa as a function of time.**

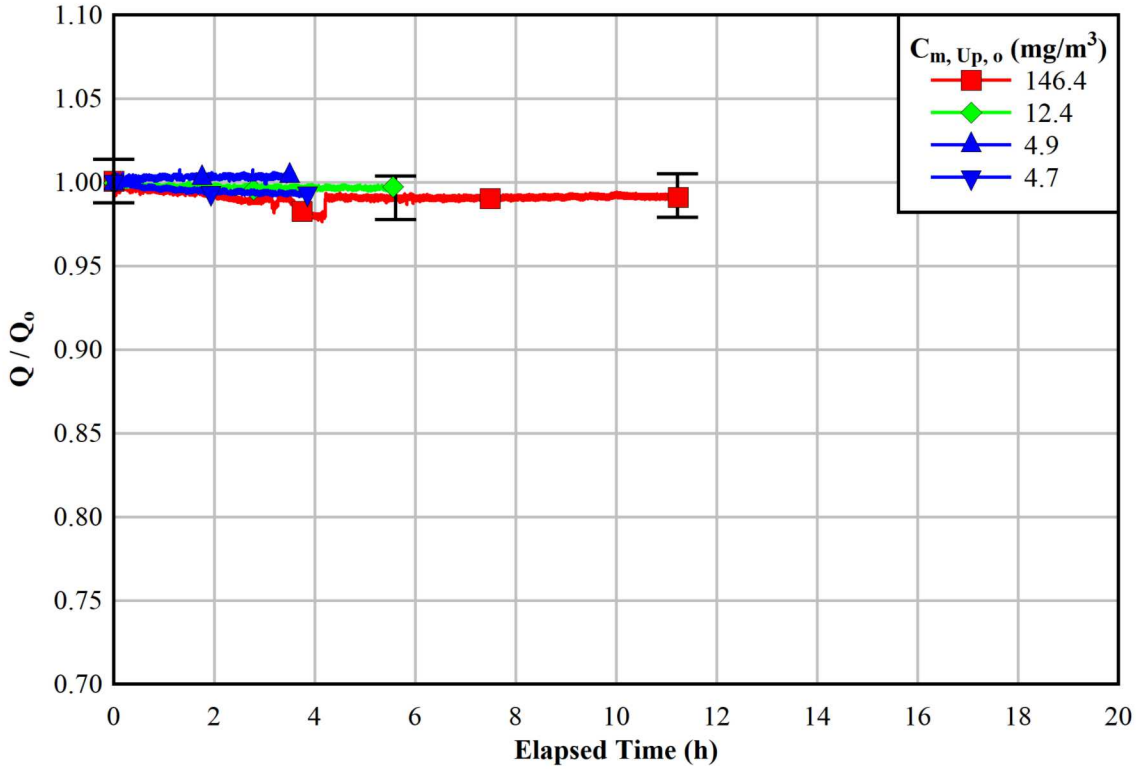

Figure 3.6 **Normalized channel gas mass flow rate for constant pressure testing at ΔP ≈ 720 kPa as a function of time.**

3.2.4 Aerosol Transmission Results

3.2.4.1 120 kPa Initial Pressure Differential

A total of six aerosol tests were conducted using the same microchannel and an initial pressure differential of about 120 kPa (see Table 3.2). The initial concentration of aerosol upstream of the crack varied from 4.0 mg/m^3 (actual) to 163 mg/m^3 (actual). The mass median diameter (MMD) of the particles analyzed by the upstream sensor ranged from 2.1 um to 2.6 µm with an average of 2.3 µm. Transient particle size information for the upstream and downstream flows are presented for all tests in Appendix A. The geometric standard deviation (GSD) ranged only from 1.9 to 2.0 with an average of 2.0. Two tests were conducted in the blowdown mode where the supply pressure could equilibrate to ambient, and four tests were conducted with the pressure differential held constant.

The ratio of the downstream to the upstream integrated mass of aerosols as a function of time for the 120 kPa blowdown and constant pressure tests are shown in Figure 3.7 and Figure 3.8, respectively. Again, the color of the data is mapped to initial aerosol concentration where blue is the lowest concentration in the range of 0.1 to 5 mg/m^3 and red is the highest concentration in the range of 100 to 500 mg/m^3.

Generally, the integrated transmission is initially low and increases asymptotically to a steady final value. The blowdown and constant pressure results are similar. The final integrated transmission ranges from 0.42 to 0.55. As seen with the mass flow rate for constant pressure of 120 kPa shown in Figure 3.4, there is also a clear correlation between integrated transmission and initial aerosol concentration shown Figure 3.7 and Figure 3.8. Increasing initial aerosol concentration leads to decreasing final integrated transmission. Aerosol deposition and plugging in the microchannel may result in decreased flow and may also enhance filtration leading to a decrease in the integrated transmission.

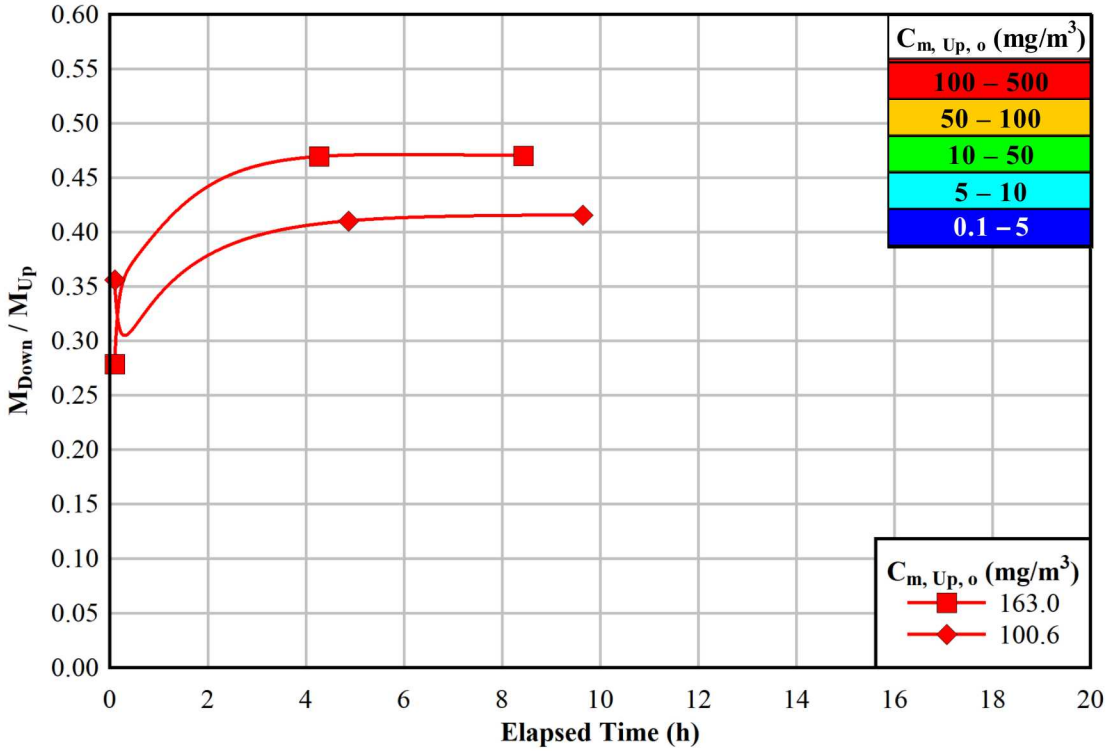

Figure 3.7 Integrated aerosol transmission for blowdown testing at $\Delta P_o \approx 120$ kPa as a function of time.

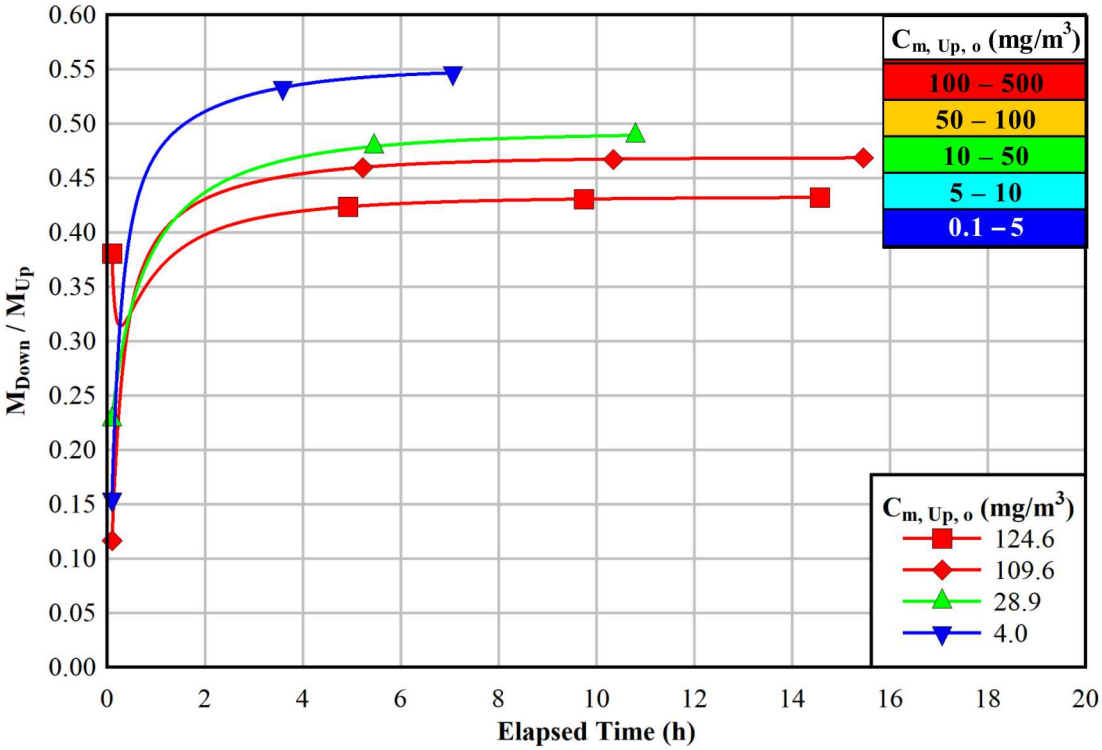

Figure 3.8 Integrated aerosol transmission for constant pressure testing at ΔP ≈ 120 kPa as a function of time.

3.2.4.2 420 kPa Initial Pressure Differential

A total of nine aerosol tests were conducted using the same microchannel and an initial pressure differential of about 420 kPa. The initial concentration of aerosol upstream of the crack varied from 1.3 mg/m^3 (actual) to 167.8 mg/m^3 (actual). The mass median diameter (MMD) of the particles analyzed by the upstream sensor ranged from 1.9 µm to 2.7 µm with an average of 2.3 µm. The geometric standard deviation (GSD) ranged from 1.9 to 2.2 with an average of 2.1. Three tests were conducted in the blowdown mode where the supply pressure was allowed to equilibrate to ambient, and six tests were conducted with the pressure differential held constant.

The ratio of the downstream to the upstream integrated mass of aerosols as a function of time for the 420 kPa blowdown and constant pressure tests are shown in Figure 3.9 and Figure 3.10, respectively. The color of the data is mapped to initial aerosol concentration where blue is the lowest concentration in the range of 0.1 to 5 mg/m^3 and red is the highest concentration in the range of 100 to 500 mg/m^3.

Again, the transmission is initially low and increases to a steady value. The blowdown and constant pressure results are similar. The final transmission ranges from 0.34 to 0.44. For this higher pressure case, there is no apparent correlation between initial aerosol concentration and final transmission with the final transmission decreasing with increasing aerosol concentration. Referring to Figure 3.5 for the constant pressure tests at 420 kPa, the final flow through the microchannel was constant with no dependence on aerosol concentration indicating no passage plugging.

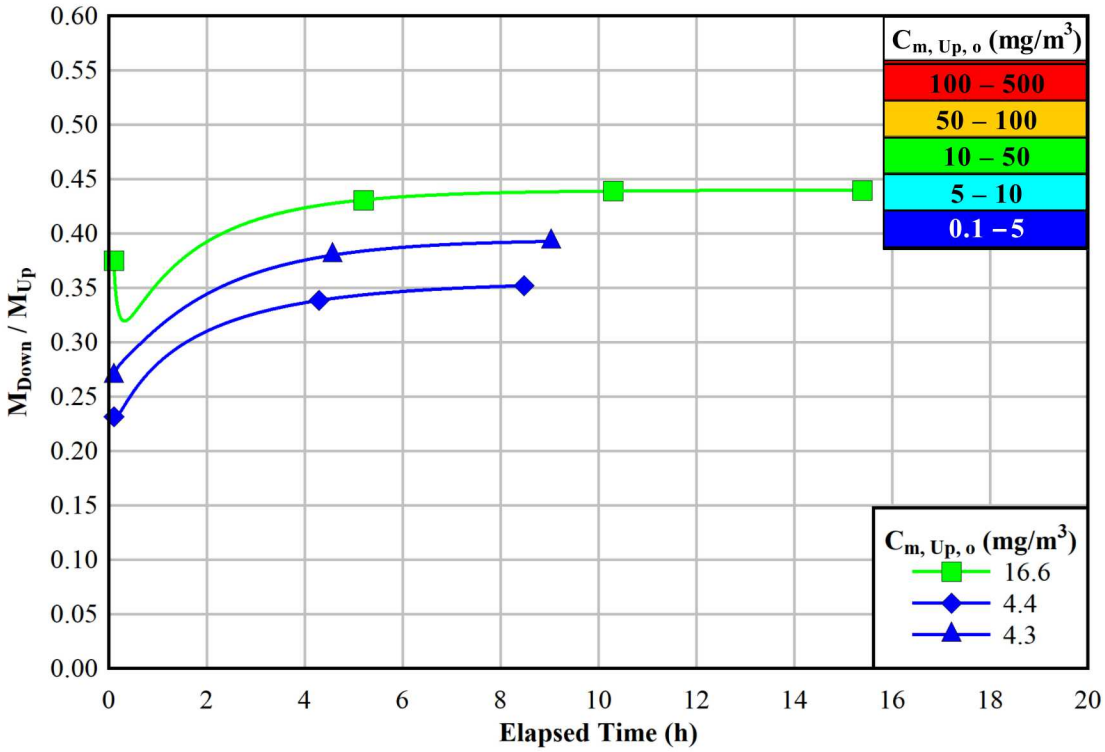

Figure 3.9 **Integrated aerosol transmission ratio for blowdown testing at $\Delta P_o \approx 420$ kPa as a function of time.**

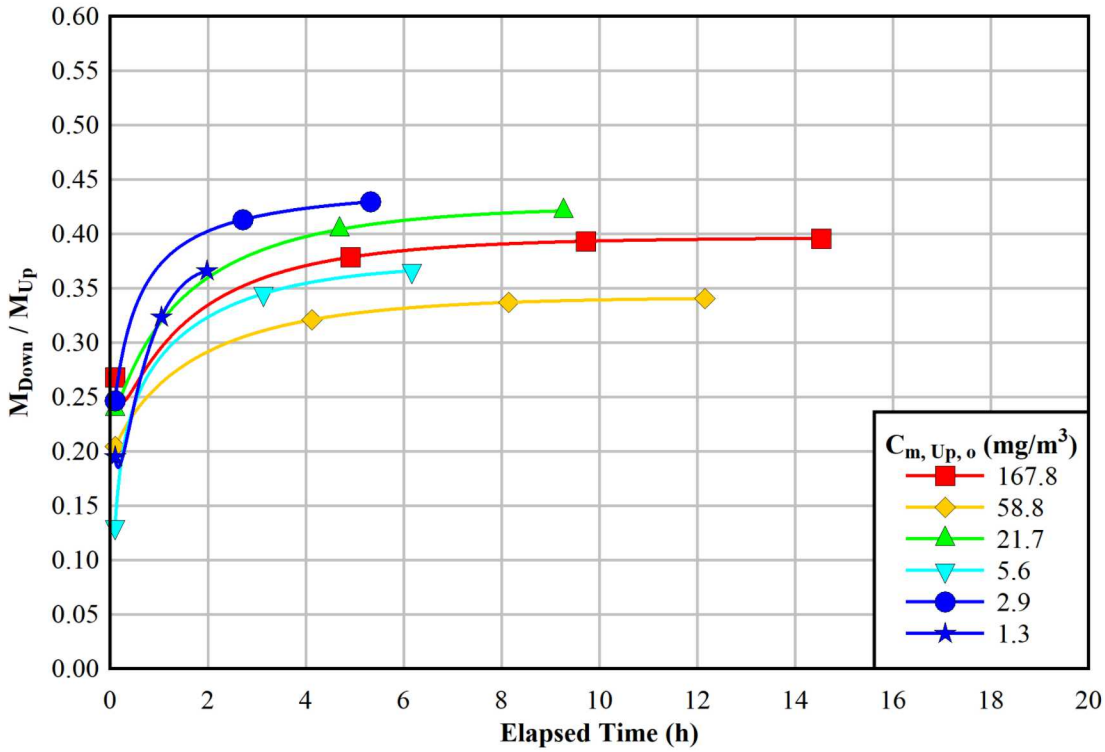

Figure 3.10 **Integrated aerosol transmission ratio for constant pressure testing at $\Delta P \approx 420$ kPa as a function of time.**

3.2.4.3 720 kPa Initial Pressure Differential

A total of seven aerosol tests were conducted using the same microchannel and an initial pressure differential of about 720 kPa. The initial concentration of aerosol upstream of the crack varied from 4.7 mg/m^3 (actual) to 153.3 mg/m^3 (actual). The mass median diameter (MMD) of the particles analyzed by the upstream sensor ranged from 2.0 µm to 4.7 µm with an average of 3.0 µm. The geometric standard deviation (GSD) ranged from 2.1 to 2.8 with an average of 2.3. Three tests were conducted in the blowdown mode where the supply pressure was allowed to equilibrate to ambient, and four tests were conducted with the pressure differential held constant.

The ratio of the downstream to the upstream integrated mass of aerosols as a function of time for the 720 kPa blowdown and constant pressure tests are shown in Figure 3.11 and Figure 3.12, respectively. The color of the data is mapped to initial aerosol concentration where blue is the lowest concentration in the range of 0.1 to 5 mg/m^3 and red is the highest concentration in the range of 100 to 500 mg/m^3.

Again, the integrated transmission is initially low and increases to a steady value. The blowdown and constant pressure results are similar. The final transmission ranges from 0.33 to 0.47. As with the 420 kPa tests, there is no apparent correlation between initial aerosol concentration and final transmission with the final transmission decreasing with increasing aerosol concentration. Referring to Figure 3.6 for the constant pressure tests at 720 kPa, the final flow through the microchannel was constant with no dependence on aerosol concentration indicating no passage plugging.

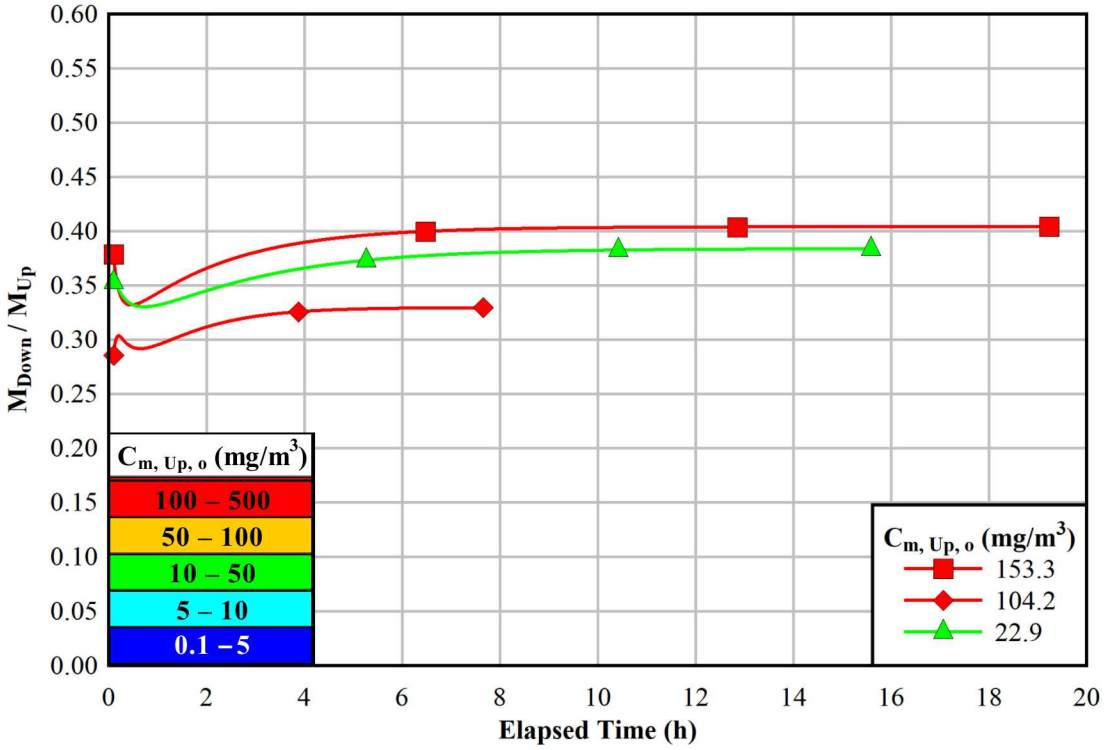

Figure 3.11 Integrated aerosol transmission ratio for blowdown testing at $\Delta P_o \approx 720$ kPa as a function of time.

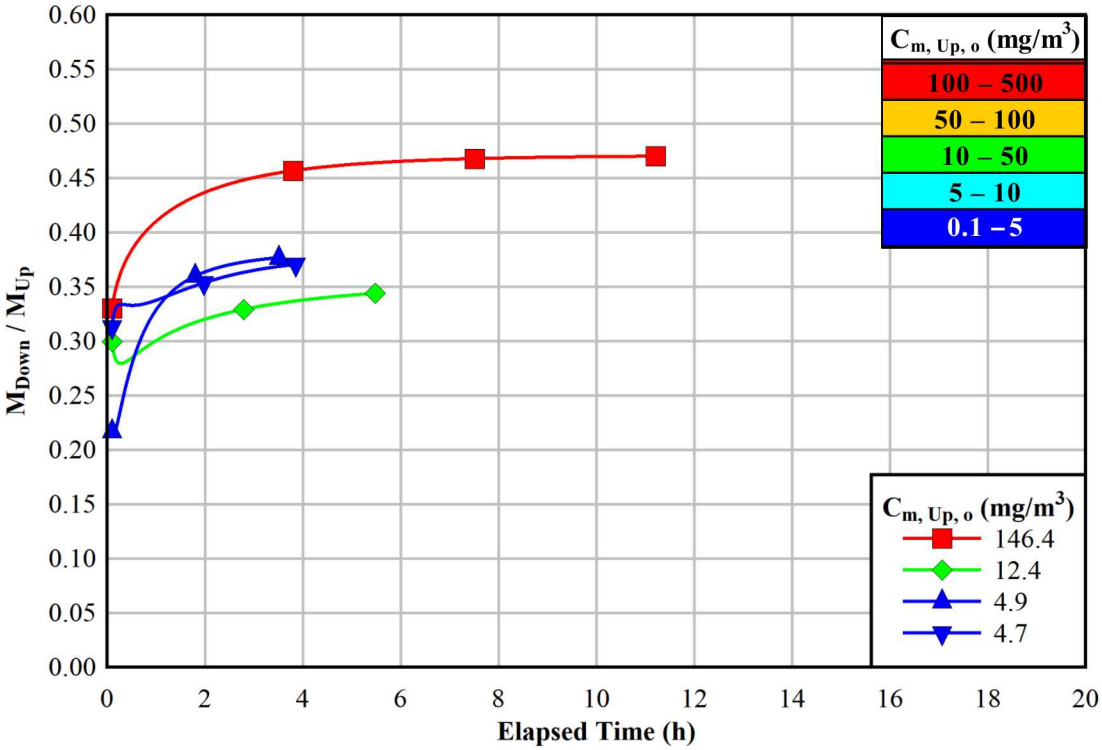

Figure 3.12 Integrated aerosol transmission ratio for constant pressure testing at ΔP ≈ 720 kPa as a function of time.

3.2.1 Aerosol Size Effects on Retention

Figure 3.13 shows the relationship between the instantaneous retention (Equations 3.1 and 3.2) and the upstream mass median diameter (MMD) as the aerosol size distribution evolved with time during the tests. These data are organized by initial pressure drop and test mode (blowdown or constant pressure). Each curve is the result of curve-fitting to all the data collected during the tests conducted with various initial aerosol concentrations. For this plot, color is used to denote initial pressure differential instead of aerosol mass concentration. The transient evolution of the upstream particle size distribution is characterized in a series of plots for all tests in Appendix A. In all cases the MMD is shown to decrease from about 3 µm at the start of the experiment to about 0.5 µm at the end. Again, a 10 µm AED particle for cerium oxide is 3.72 µm.

In general, the retention is highest when the MMD is greatest at the beginning of a test and drops as the MMD decreases. Especially for the constant pressure mode, the rate of the initial decrease of retention at the start of the test seems correlated with the pressure differential. Of the three pressure differentials, the retention for the lowest differential of 120 kPa decreases the most with decreasing MMD. The retention for the highest differential of 720 kPa decreases the least with decreasing MMD. The differential of 420 kPa is bounded by the other two.

When the MMD drops below 1 µm, the behavior in the blowdown mode and the constant pressure mode appears to deviate. In the constant pressure mode, the retention continues to drop as the MMD drops below 1 µm. However, in the blowdown mode the retention passes a minimum and increases at the small MMD.

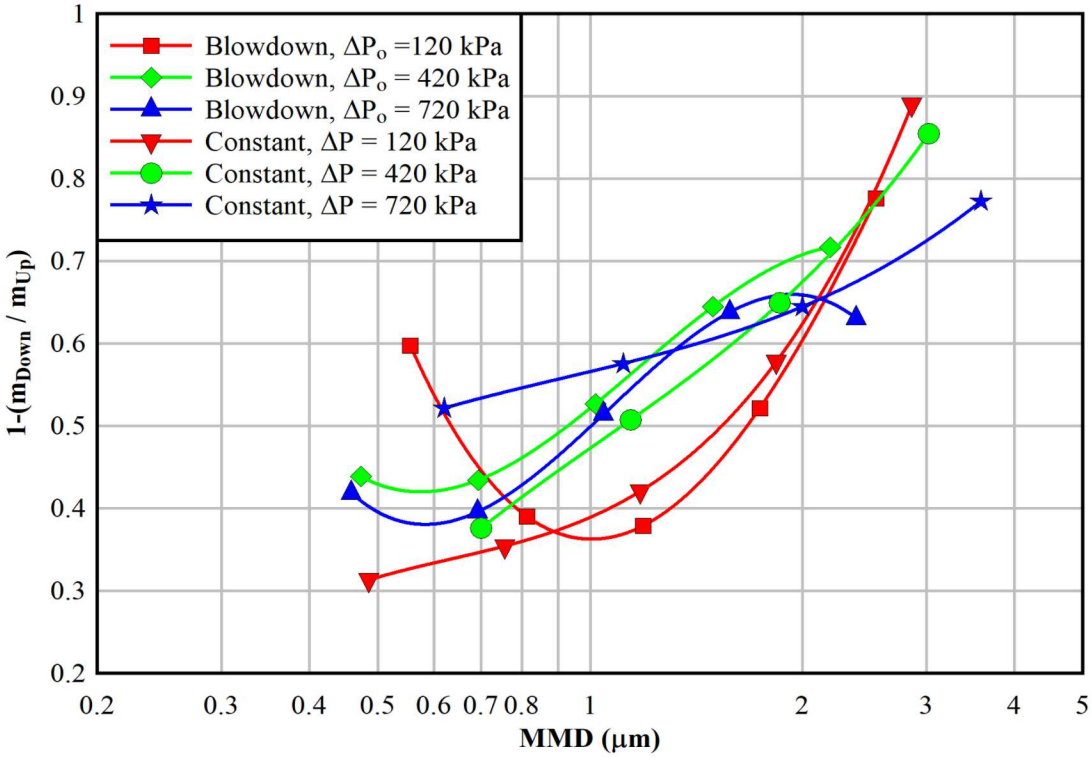

Figure 3.13 Aerosol retention for all testing as a function of upstream MMD.

3.2.2 Post-Test Images

Figure 3.14 shows the aerosols deposited in the crack after two different constant pressure tests for ΔP = 120 kPa. Flow is from the bottom of the photos to the top of the photos. Note that the unmodified gage block has been rotated 180 degrees in the photographs to align both blocks with the flow direction while exposing the microchannel. When assembled, the superimposed positive "+" and negative "–" signs would match and touch on the two blocks. Most of the aerosol deposits are on the leading, upstream edge of the slot orifice. Streaking from the displacement of larger aerosol agglomerates appears to be more pronounced in the photo of the May 27, 2020 test, likely because the initial aerosol concentration was almost four times higher.

Figure 3.14 Visual inspection of the disassembled microchannel after testing.

Figure 3.15 shows three scanning electron microscope (SEM) images of increasing magnification for the test conducted on July 1, 2020. This test also had a constant pressure drop of $\Delta P = 120$ kPa as in the previous photographs, but the initial upstream aerosol mass concentration was considerably lower at $C_{m,\,Up,\,o} = 4.0$ mg/m^3. The image on the left shows a closeup of the left side of the leading edge of the slot orifice. Notice the accumulation of aerosols starting just beyond the leading edge. The image in the middle shows an intermediate magnification, and the image on the right shows a detailed zoom where the agglomerations are revealed to be constructed of individual particles

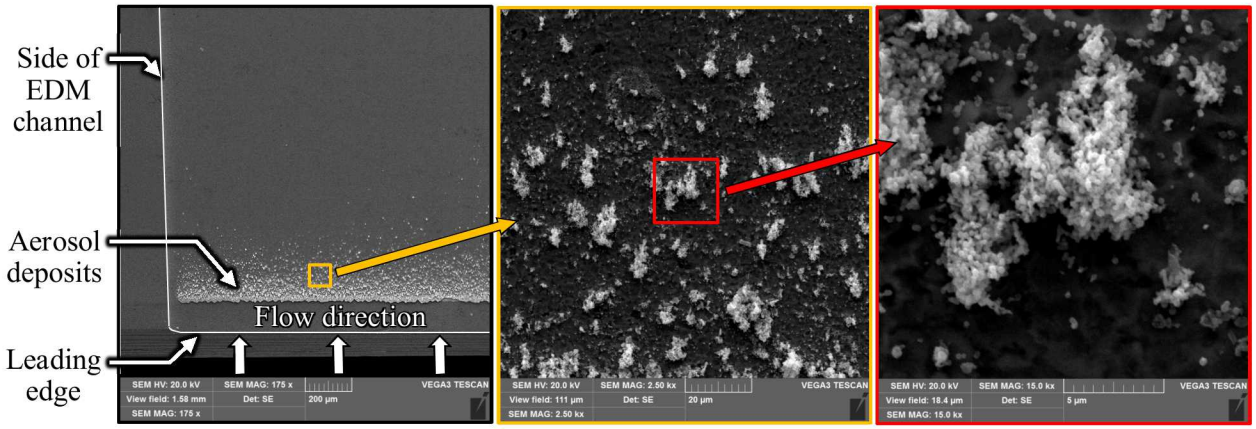

Figure 3.15 SEM images of CeO_2 deposits in the microchannel from testing on July 7, 2020.

This page intentionally blank.

5 SUMMARY

Using a microchannel with a cross-section of 12.7 mm × 28.9 μm and a flow length of 8.86 mm, a total of twenty-two aerosol-laden tests were conducted for three nominal initial pressure drops (120 kPa, 420 kPa, and 720 kPa) and two test modes (blowdown and constant pressure) over a wide range of initial upstream aerosol concentrations (1.3 mg/m^3 to 168 mg/m^3). With a channel height more akin to the largest dimension of a potential SCC and without any tortuosity, this microchannel represents a relatively conservative simplification of a SCC in a dry storage canister for SNF. In the blowdown mode, the supply pressure was allowed to equilibrate to ambient, while in the constant pressure mode, the pressure differential across the channel was held constant. A summary of the aerosol transmission results is presented in Table 5.1. The integrated aerosol transmission only varied from 0.33 to 0.55 even though the initial aerosol mass concentration changed by two orders of magnitude. Because aerosol mass transmission largely occurred at the beginning of the tests, there was no discernable difference in the transmission between the blowdown tests and the tests conducted at constant pressure.

Table 5.1 Summary of results.

			Upstream Initial Conditions				
Date	**Test Mode**	**ΔP_o (kPa)**	**C_m (mg/m^3)**	**$C_{m,STP}$ (mg/m^3)**	**MMD (μm)**	**GSD**	**Integrated Transmission**
4/29/2020	Blowdown	121	163.0	80.7	2.3	2.0	0.470
4/23/2020	Blowdown	125	100.6	49.2	2.6	1.9	0.416
5/27/2020	Constant Press.	116	124.6	62.1	2.1	1.8	0.432
6/3/2020	Constant Press.	120	109.6	54.7	2.5	2.0	0.468
6/9/2020	Constant Press.	118	28.9	14.3	2.3	2.0	0.489
7/1/2020	Constant Press.	118	4.0	2.0	2.2	1.9	0.546
7/24/2020	Blowdown	417	16.6	3.4	2.0	2.2	0.440
7/17/2020	Blowdown	417	4.4	0.9	2.2	2.0	0.352
7/23/2020	Blowdown	417	4.3	0.9	2.0	2.0	0.393
7/6/2020	Constant Press.	418	167.8	33.5	2.7	2.0	0.396
7/22/2020	Constant Press.	417	58.8	11.7	2.6	2.1	0.340
7/8/2020	Constant Press.	417	21.7	4.3	2.7	2.0	0.421
7/20/2020	Constant Press.	417	5.6	1.1	2.3	2.1	0.366
7/16/2020	Constant Press.	417	2.9	0.6	1.9	2.1	0.429
7/15/2020	Constant Press.	417	1.3	0.3	2.7	1.9	0.366
5/5/2020	Blowdown	726	153.3	19.6	2.3	2.1	0.404
4/20/2020	Blowdown	740	104.2	13.0	2.1	2.2	0.329
7/29/2020	Blowdown	714	22.9	2.9	2.0	2.3	0.384
5/20/2020	Constant Press.	713	146.4	18.3	4.7	2.7	0.470
6/24/2020	Constant Press.	713	12.4	1.5	3.7	2.1	0.344
6/29/2020	Constant Press.	715	4.9	0.6	3.3	2.1	0.377
6/18/2020	Constant Press.	715	4.7	0.6	2.5	2.2	0.370

Because of the relatively large channel height and lack of tortuosity, this range of aerosol transmission is presented as a conservative estimate for through-wall transmission in the determination of respirable

release fractions for SCC consequence analyses. These values should not be confused with a canister-to-environment respirable release fraction but are instead meant to be one fraction applied to a source term in a consequence analysis. Further studies are needed to estimate the transient depletion of aerosols within a canister during normal storage conditions to couple with these results for respirable release fraction estimates from the canister interior to the environment.

This test series has demonstrated a unique capability to directly measure aerosol transmission through SCC-like geometries at pressure differentials of interest for the long-term storage of SNF. The test apparatus and associated instrumentation have shown an excellent robustness and accuracy for these characterizations.

Additional testing is planned to approach more prototypic SCCs. Using the successful techniques summarized in this report with EDM blocks, a microchannel with roughly one-third the depth of the channel in this study (~10 μm or 0.0004 in.) is planned to represent the smaller, interior dimension of typical SCCs. A diverging channel with starting dimensions of ~10 μm linearly transitioning to ~30 μm is also under consideration. An additional complexity being considered is a slot orifice with a single offset step. This geometry will allow the introduction of a simple and known tortuosity in the flow path. Finally, the growth of realistic stress corrosion cracks has been successfully demonstrated for accelerated laboratory conditions [EPRI, 2018]. The method requires creating a tensile stress field through-wall in a specimen and exposing it to a potassium tetrathionate ($K_2S_4O_6$) solution for a relatively short period. Plans to mount and test these types of representative cracks in the existing apparatus are under review.

6 REFERENCES

Durbin, S.D., E.R. Lindgren and R.J.M. Pulido, "Measurement of Particulate Retention in Microchannel Flows", SAND2018-10522R, Sandia National Laboratories, Albuquerque, New Mexico, September (2018).

EPRI, "Flaw Growth and Flaw Tolerance Assessment for Dry Cask Storage Canisters," EPRI 3002002785 Electric Power Research Institute, Palo Alto, CA, October (2014).

EPRI., "Dry Cask Storage Welded Stainless Steel Canister Breach Consequence Analysis Scoping Study," EPRI 3002008192, Electric Power Research Institute, Palo Alto, CA, November (2017).

Hanson, B.D., R.C. Daniel, A.M. Casella, R.S. Wittman, W. Wu (BSC), P.J. MacFarlan, and R.W. Shimskey, "Fuel-In-Air FY07 Summary Report," PNNL-17275, Pacific Northwest National Laboratory, Richland, Washington, September (2008).

Lewis, S., "Solid Particle Penetration into Enclosures", J. Hazardous Materials, *43,* 195-216, (1995).

Liu, D-L.and W.W. Nazaroff, "Modeling Pollutant Penetration Across Building Envelopes," **Atmos. Environm**., ***35,*** 4451-4462, (2001).

Liu, D-L. and W.W. Nazaroff, "Particle Penetration Through Building Cracks," **Aerosol Science and Technology**, ***37***, 565-573, (2003).

Meyer, R.M., S. Suffield, E.H. Hirt, J.D. Suter, J.P. Lareau, J.W. Zhuge, A. Qiao, T.L. Moran, and P. Ramuhalli, "Nondestructive Examination Guidance for Dry Storage Casks," PNNL-24412 Rev. 1, Pacific Northwest National Laboratory, Richland, Washington, September (2016).

Mosely, R.B., D.J. Greenwell, L.E. Sparks, Z. Guo, W.G. Tucker, R. Fortmann, C. Whitfield, "Penetration of Ambient Fine Particles into the Indoor Environment," **Aerosol Science and Technology**, ***34***, 127-136, (2001).

NRC, "Spent Fuel Transportation Risk Assessment," United States Nuclear Regulatory Commission, NUREG-2125, May (2012).

Powers, D.A., "Aerosol Penetration of Leak Pathways – An Examination of the Available Data and Models," SAND2009-1701, Sandia National Laboratories, Albuquerque, NM, April (2009).

Sanders, T.L., K.D. Seager, Y.R. Rashid, P.R. Barrett, A.P. Malinauskas, R.E. Einziger, H. Jordan, T.A. Duffey, S.H. Sutherland, and P.C. Reardon "A Method for Determining the Spent-Fuel Contribution to Transport Cask Containment Requirements," SAND90-2406, Sandia National Laboratories, Albuquerque, NM, November (1992).

Schindelholz, E., C. Bryan, and C. Alexander, "FY17 Status Report: Research on Stress Corrosion Cracking of SNF Interim Storage Canisters," SAND2017-10338R, Sandia National Laboratories, Albuquerque, NM, August (2017).

This page intentionally blank.

APPENDIX A TRANSIENT PARTICLE SIZE DISTRIBUTIONS

The upstream and downstream transient particle sizes for D_{16}, D_{50} (*i.e.* MMD), and D_{84} for mass are presented in this appendix for all tests. Sixteen percent of the particles have a mass less than D_{16}. Similarly, eighty-four percent of the particles have a mass less than D_{84}. The colormap for initial, upstream aerosol mass concentration defined in the report is adopted for these results (Red for $500 \geq C_{m, Up, o} > 100$ mg/m^3, orange for $100 \geq C_{m, Up, o} > 50$ mg/m^3, green for $50 \geq C_{m, Up, o} > 10$ mg/m^3, turquoise for $10 \geq C_{m, Up, o} > 5$ mg/m^3, and blue for $5 \geq C_{m, Up, o} > 1$ mg/m^3).

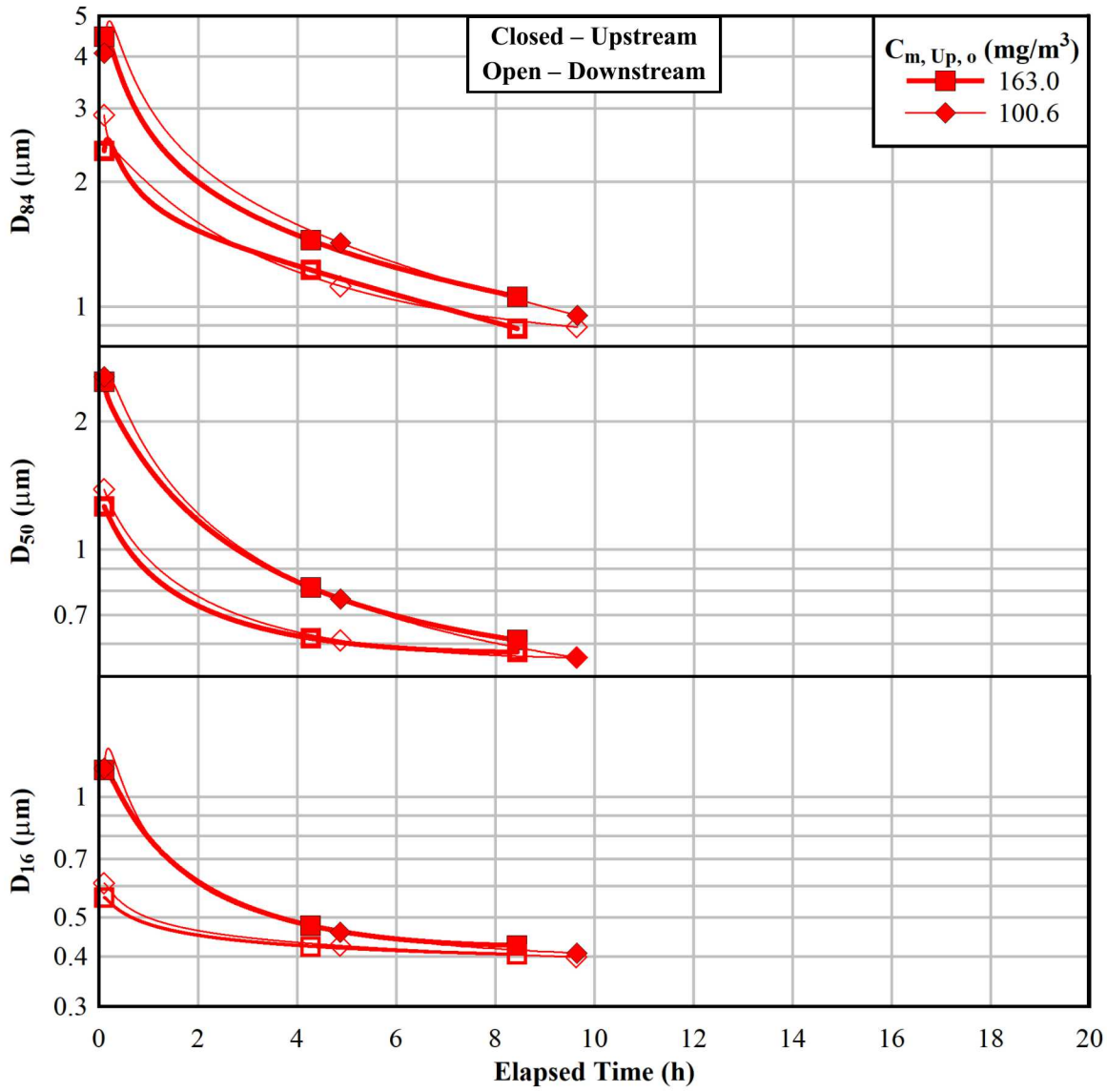

Figure A.1 Particle sizes for ΔP_o = 120 kPa blowdown tests.

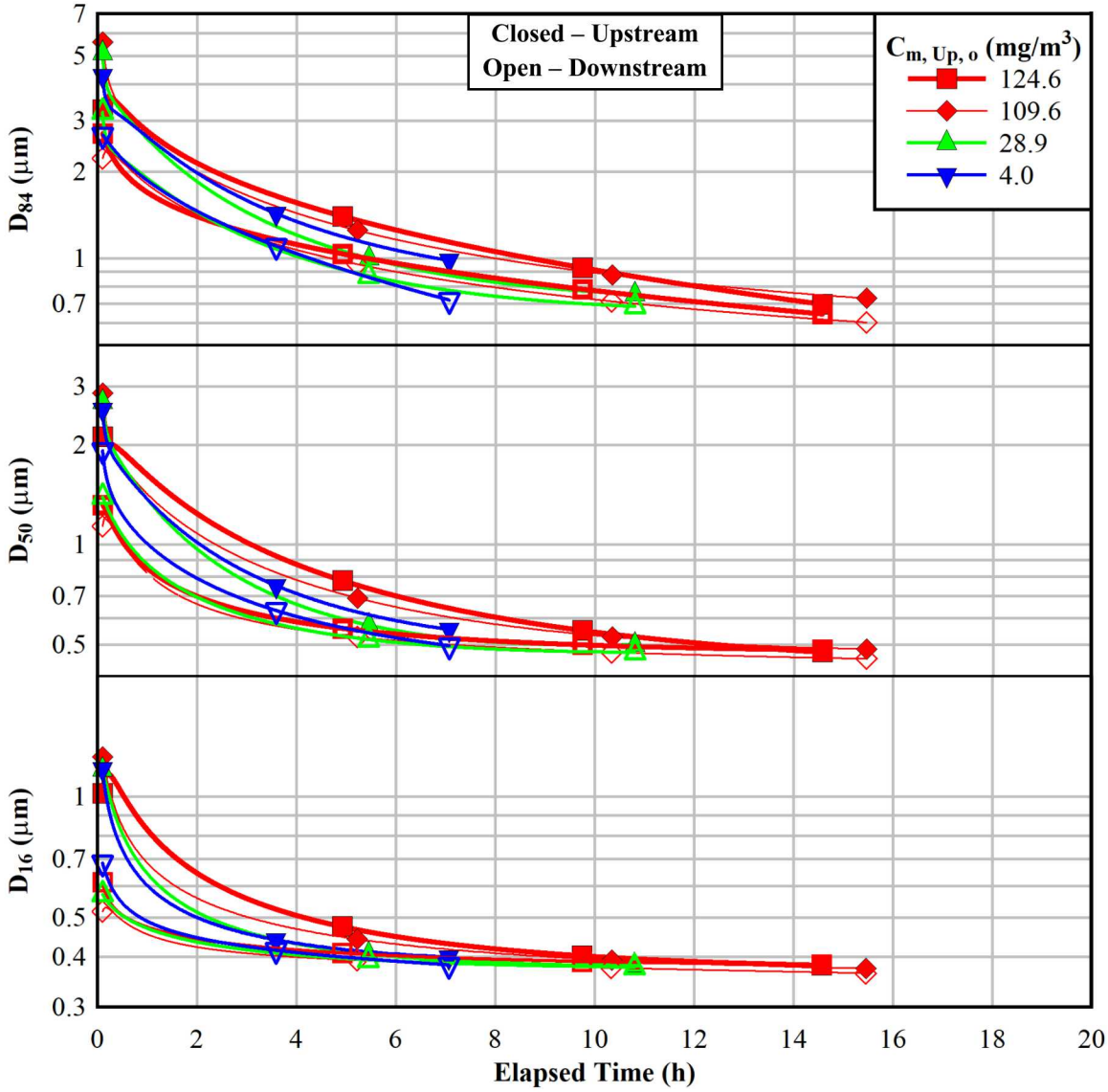

Figure A.2 Particle sizes for ΔP = 120 kPa constant pressure tests.

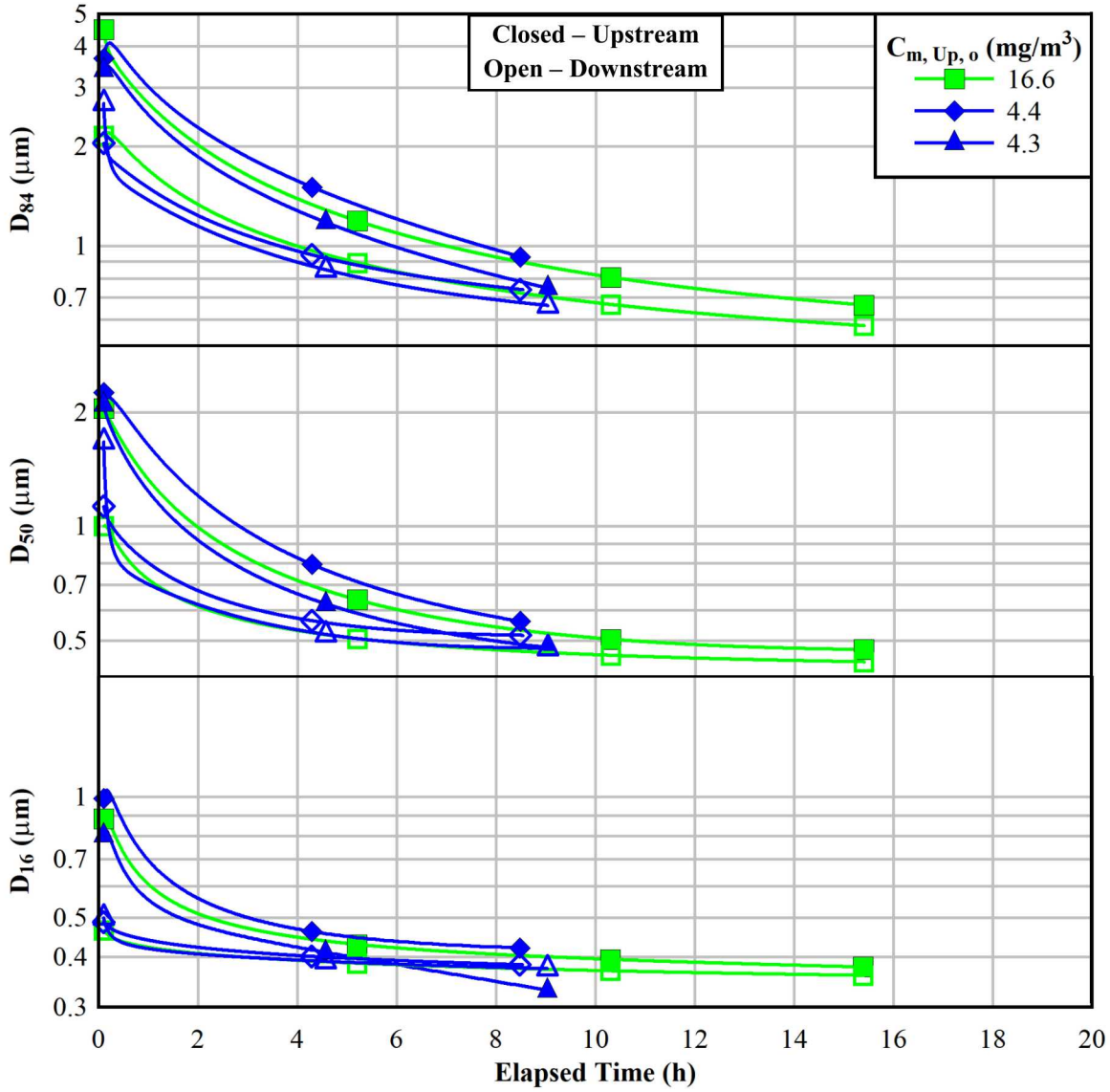

Figure A.3 Particle sizes for ΔP_o = 420 kPa blowdown tests.

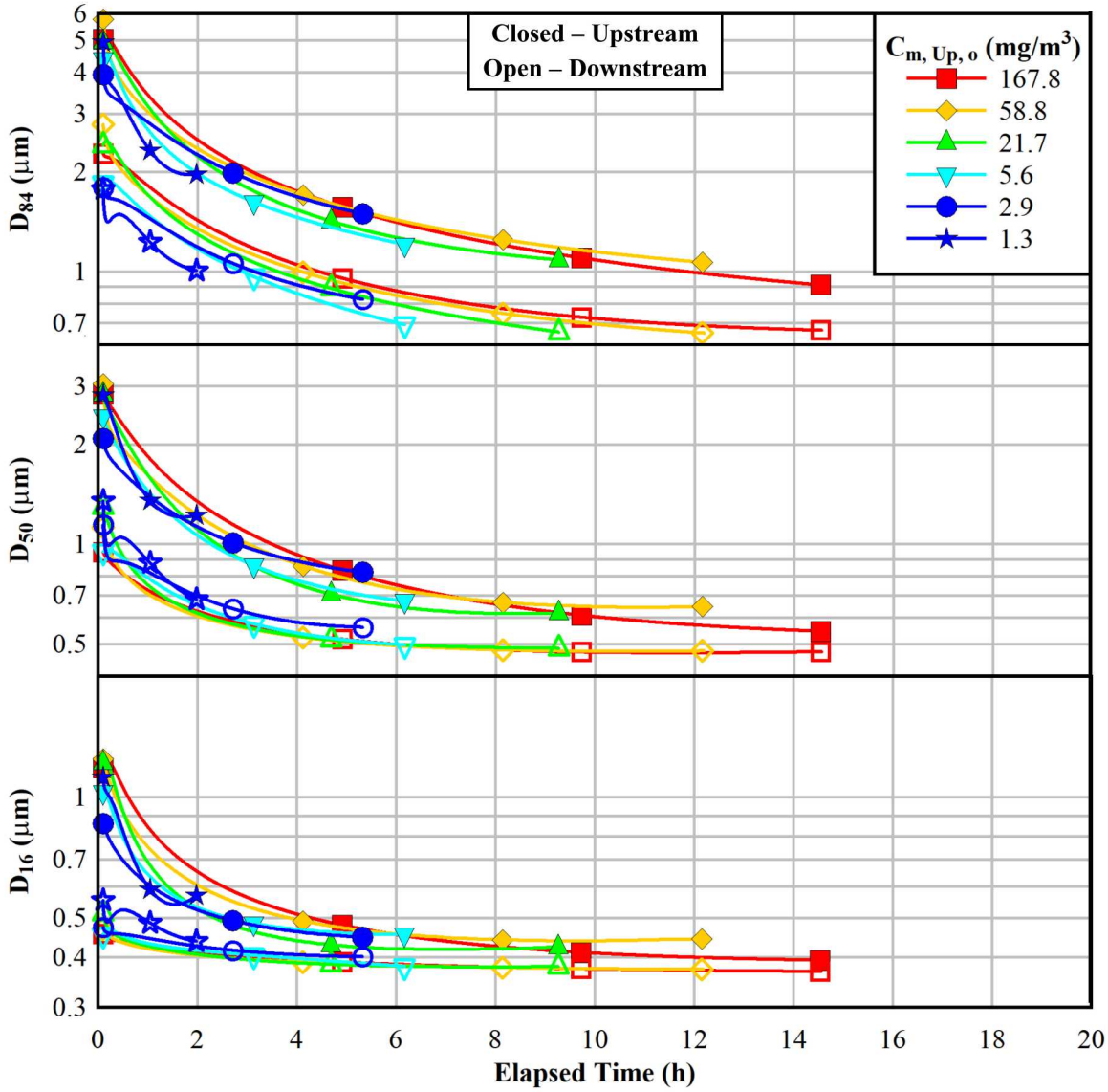

Figure A.4 Particle sizes for ΔP = 420 kPa constant pressure tests.

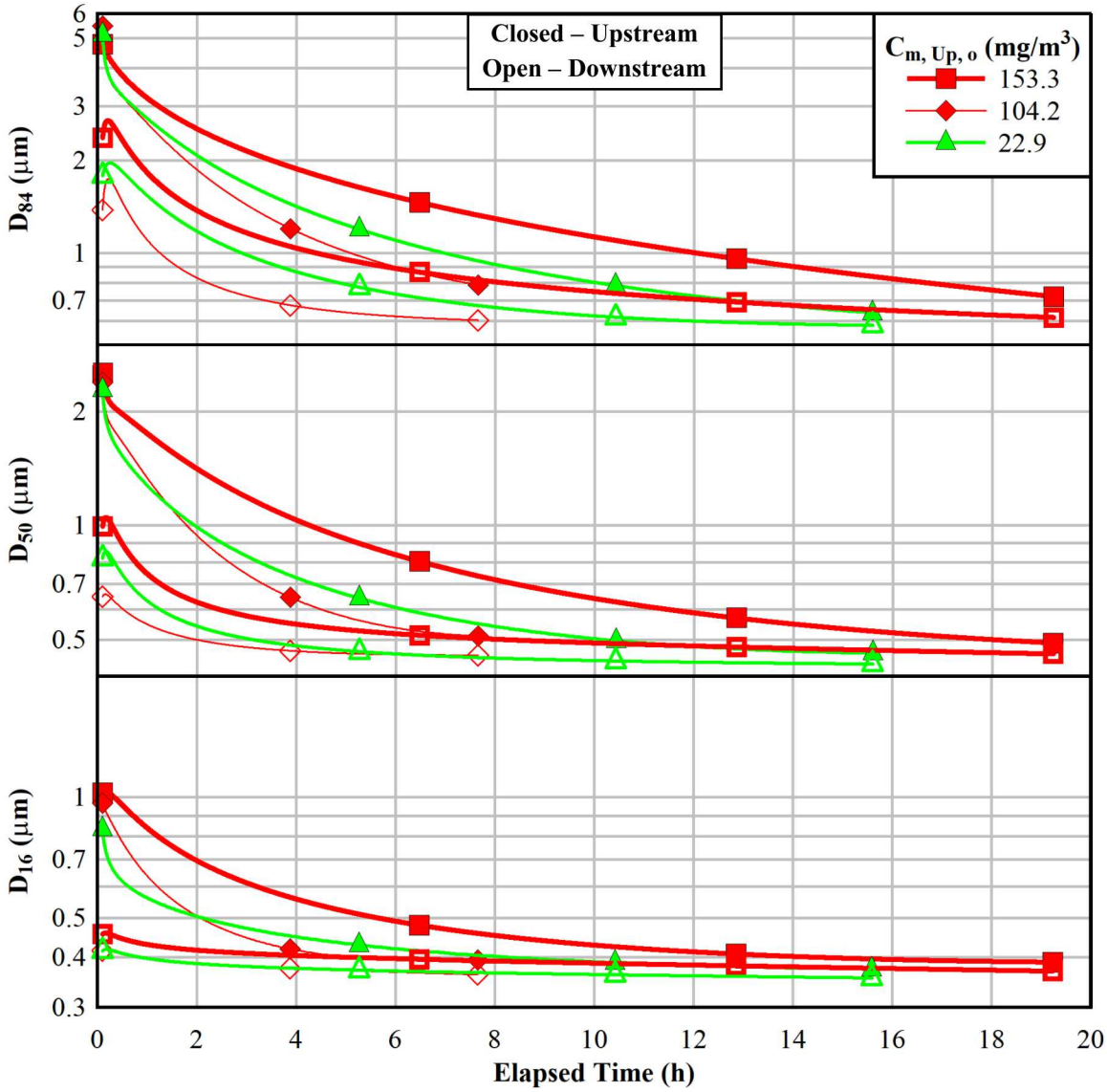

Figure A.5 Particle sizes for ΔP_o = 720 kPa blowdown tests.

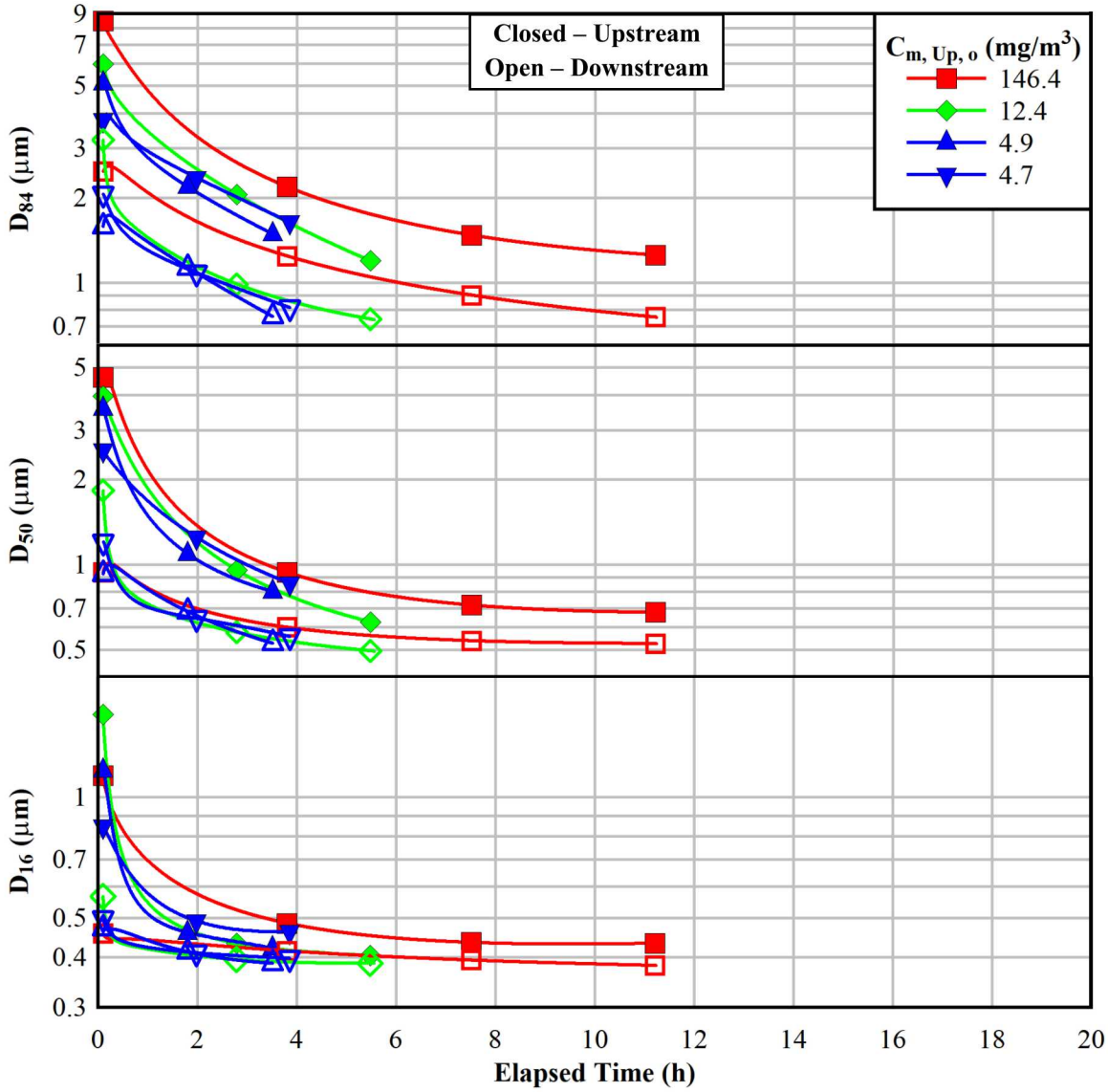

Figure A.6 Particle sizes for ΔP = 720 kPa constant pressure tests.

Sandia National Laboratories